Journal of African Earth Sciences 235 (2026) 105978

Contents lists available at ScienceDirect

Journal of African Earth Sciences

journal homepage: www.elsevier.com/locate/jafrearsci

Evolution of the Suhum Basin of the Rhyacian Birimian terrane in Ghana: Insight from paraschist and orthoamphibolite

Daniel Kwayisi [a], Susanna S. Boateng [a,*], Naa A. Agra [a], Solomon Anum [b], Raymond W. Kazapoe [c], Abigail E. Ayikwei [a], Chris Y. Anani [a], Daniel K. Asiedu [a]

[a] Department of Earth Science, University of Ghana, P. O. Box LG 58, Legon, Accra, Ghana
[b] Geological Survey Authority of Ghana, Accra, Ghana
[c] Department of Geological Engineering, University for Development Studies, Nyankpala, Ghana

ARTICLE INFO

Handling Editor: DR Damien Delvaux

ABSTRACT

We present petrographical and geochemical data of paraschists and orthoamphibolite from the Suhum-Akwadum area of the Suhum Basin, Ghana, to determine their provenance, petrogenesis, and tectonic setting, and discuss the crustal evolution of the Rhyacian Birimian terrane of the West African Craton. The amphibolite exhibits trace element signatures similar to those of subalkaline basalts. Two main geochemical groups are present: (1) dominant arc-rocks with negative Nb-Ta, Ti, low Nb/Th and high La/Nb, and (2) subordinate enriched mid-ocean ridge basalts characterised by moderate to high TiO_2, positive Ta and high Nb/Th value. These compositions are interpreted as formation in a supra-subduction zone setting. The schists are geochemically classified as shales and wackes and have <60 CIA, <70 CIW, moderate to high Al_2O_3/TiO_2 and Na_2O/K_2O, low SiO_2/Al_2O_3, La/Sc, and Ti/Zr values. These geochemical signatures are consistent with low chemical weathering intensity, immature to moderately mature sediments and deposition in an active continental margin setting with sediments sourced from greenstone and granitoid-gneiss complexes of the Rhyacian Birimian terrane. Therefore, the current and previous geochemical data confirm the presence of an arc tectonic setting in the formation of the metasedimentary basins of the Birimian terrane. The overall geochemical data suggest that the greenstones and metasedimentary rocks formed during an orogenic event related to an arc environment where subduction zone components contributed to the generation of their parental magmas and sedimentation. This finding is consistent with the onset of "modern-style" subduction-related processes during the Archean-Paleoproterozoic transitional period.

1. Introduction

The southeastern part of the West African Craton (WAC) is composed mainly of the Rhyacian Birimian terrane of greenstone belts, metasedimentary basins and granitoid-gneiss complexes (Fig. 1) (Sakyi et al., 2014; Nunoo et al., 2022; Amponsah et al., 2023; Atanga et al., 2023). Other components of the WAC include the Archean domains to the west (Kouamelan et al., 2015; Rollinson, 2016) and Neoproterozoic Pan-African belts that surround the WAC to the east (Nude et al., 2015; Kwayisi et al., 2022a,b, 2023, 2024). The Rhyacian Birimian terrane archived the evolution of the southeastern portion of the WAC during the Eburnean orogeny between 2.2 and 2.0 Ga (Abouchami et al., 1990; Sakyi et al., 2014, 2018, 2019, 2020; Asiedu et al., 2019; Baratoux et al., 2019; Agra et al., 2023; Amponsah et al., 2023; Atanga et al., 2023). The most widely accepted evolutionary model for the Rhyacian Birimian terrane is that of subduction-accretion in either arc-back-arc or supra-subduction setting (Dampare et al., 2008; Senyah et al., 2016; Sakyi et al., 2018; McFarlane et al., 2019). The Rhyacian Birimian terrane is exposed in Ghana as six granitoid-greenstone belts separated by metasedimentary basins (Fig. 2a; Agyei-Duodu et al., 2009). The greenstone belts are Lawra, Bole-Nangodi, Bui, Sefwi, Ashanti and Kibi-Winneba belts, with the metasedimentary basin being Maluwe, Sunyani, Kumasi, Cape Coast and Suhum basins (Fig. 2a) (Asiedu et al., 2019; Sakyi et al., 2019; Agra et al., 2023; Kazapoe et al., 2022, 2023; Kwayisi et al., 2025). Four broad types of granitoids intrude the greenstone belts and metasedimentary basins, and these are Dixcove, Cape Coast, Winneba, and Bongo-type granitoids (Anum et al., 2015; Abitty et al., 2016; Amponsah et al., 2023; Sakyi et al., 2024).

* Corresponding author.
E-mail address: suzanneadiamah@gmail.com (S.S. Boateng).

https://doi.org/10.1016/j.jafrearsci.2025.105978
Received 9 May 2025; Received in revised form 9 November 2025; Accepted 12 December 2025
Available online 13 December 2025

Available petrographic, major and trace element, and Rb-Sr and Sm-Nd data for the metasedimentary rocks from the Ashanti, Lawra, Sefwi, and Bole-Nangodi belts, and Kumasi basin suggest deposition in an active continental margin characterised by subduction-accretion processes, with sediments sourced from the greenstone and granitoid-gneiss complexes of the Rhyacian Birimian terrane (Roddaz et al., 2007; Asiedu et al., 2009, 2017, 2019; Manu et al., 2013; Sakyi et al., 2019; Brako et al., 2022). Until recently, the Suhum Basin had received very little research attention. Detailed petrographical and geochemical studies, including isotopic and geochronological studies of granitoids in the Suhum Basin, indicate juvenile mantle rocks with significant recycled Archean crust formed during subduction-accretion processes in a supra-subduction (Amponsah et al., 2023). However, paraschists and amphibolites that occur as pockets within the Suhum Basin have not been documented. Sedimentary rocks and their metamorphosed equivalents are important in crustal evolutionary studies because their petrographic features and geochemical signatures serve as archives for provenance, source area paleoweathering, paleoclimatic conditions, and paleotectonic settings (Bhatia and Crook, 1986; Nesbitt and Young, 1982; Verma and Armstrong-Altrin, 2016). It is important to note that the current understanding of continental crust mainly stems from studies on the geochemistry of sedimentary rocks (Taylor and McLennan, 1985; Condie, 1993; Roddaz et al., 2007).

Therefore, this research aimed to analyse the petrography and major and trace-element geochemistry of the paraschists and amphibolite from the Suhum-Akwadum area of the Suhum Basin. The objectives of this study are (i) to determine the protolith of the schists and amphibolite, (ii) to discuss the effect of weathering/metamorphism/alteration on the compositions of the schists and the amphibolite, (iii) to interpret these data in relation to source rock composition, provenance, and tectonic setting of the depositional basin of the schists, and petrogenesis, and tectonic setting of the amphibolite; and iv) to compare the data to other Birimian terranes of Ghana to put constraints on the crustal evolution of the Suhum Basin in the context of the Rhyacian Birimian terrane of the West African Craton.

1.1. Geological setting

The Rhyacian Birimian terrane, also known as the Baoulé-Mossi Domain, outcrops east of the Leo-Man Shield of the West African Craton (Fig. 1). It extends from the western half of Ghana into countries such as Côte D'Ivoire, southern Mali, Senegal, Burkina-Faso and west of Niger (Fig. 1). The Rhyacian Birmian terrane which formed during the 2.2–2.0 Eburnean tectono-metamorphic events, is comprised of greenstone belts, metasedimentary basins, and granitoid-gneiss complexes (Sakyi et al., 2014, 2020; Anum et al., 2015; Nunoo et al., 2022; Amponsah et al., 2023; Atanga et al., 2023). The metasedimentary rocks comprise phyllites and graywackes, while the greenstones are composed of basalts, andesites, and rhyolite (Asiedu et al., 2009; Manu et al., 2013; Sakyi et al., 2020). Chemical units comprising chert, carbonate rocks and manganese often mark the boundary between the greenstones and metasedimentary rocks (Nyame and Beukes, 2006; Nyame, 2008). The granitoid-gneiss complexes intrude the greenstone belt (known as belt-type) and the metasedimentary basins (referred to as basin-type) (Sakyi et al., 2014, 2019; Nunoo et al., 2022; Amponsah et al., 2023). The greenstone belts and metasedimentary basins are contemporaneous lateral facies equivalents formed in an arc-back-arc or supra-subduction environment (Leube et al., 1990; Dampare et al., 2008; Baratoux et al., 2011; Sakyi et al., 2018; Asiedu et al., 2019; McFarlane et al., 2019). However, other researchers have proposed intra-continental rifting or plume setting for the greenstone belts (Abouchami et al., 1990; Leube et al., 1990; Boher et al., 1992; Agra et al., 2023). The greenstone belts are of both tholeiitic and calc-alkaline signatures, with the tholeiites considered older than the calc-alkaline series (Baratoux et al., 2011; Sakyi et al., 2020). These contradictory interpretations of the evolution of the Birimian Paleoproterozoic rocks have attracted a lot of attention for nearly a century.

As stated earlier, the Rhyacian Birimian terrane exposed in Ghana is characterised by six greenstone belts (Fig. 2a). The Kibi-Winneba greenstone belt (Fig. 2a) in southeastern Ghana is characterised by volcanic lobes, made up of basaltic flows, andesitic lavas, amphibolite, pyroclastics with granite–diorite plutonic suites and metasedimentary rocks (Anum et al., 2015). Mafic plutonic bodies also intrude on parts of the belt. This belt displays very similar lithological and structural

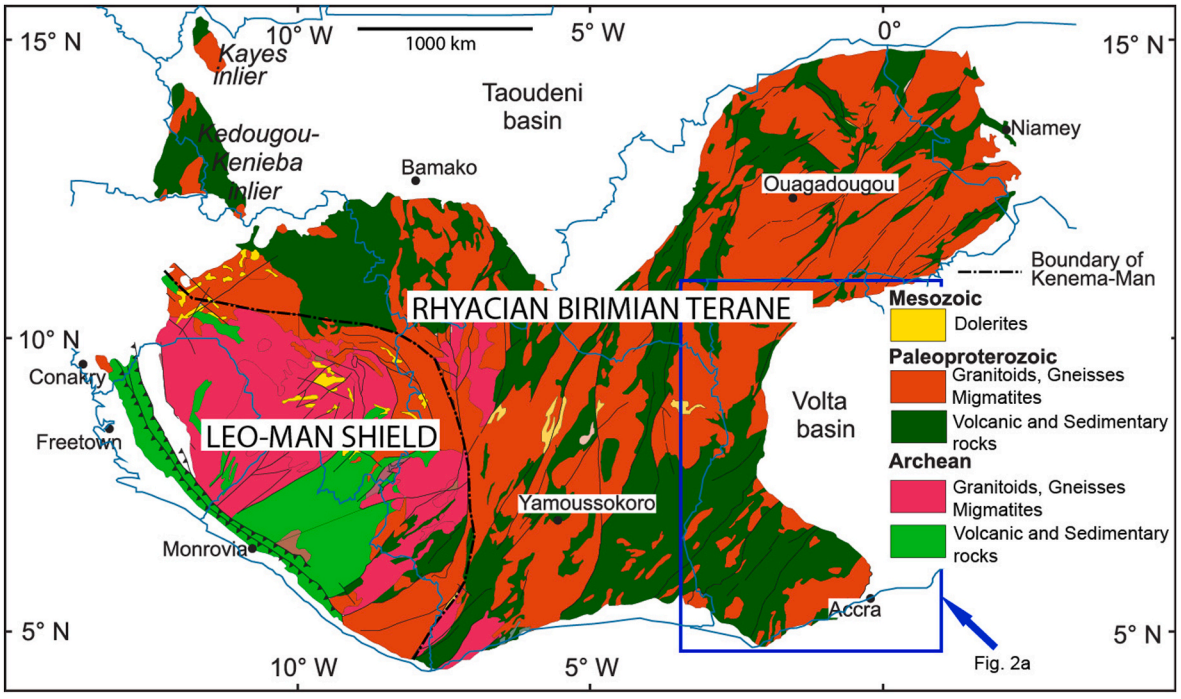

Fig. 1. Geological map of Southern West African Craton (After Milesi et al., 1992).

characteristics to the greenstone belts located in western Ghana. According to Anum et al. (2015), both the Birimian metavolcanic and metasedimentary rocks of the Kibi-Winneba belt are intruded by different types of granitoids. The most obvious feature in all the outcrops within this terrane is the presence of mafic enclaves, made up mostly of amphibolite and gabbro. The Kibi-Winneba belt is separated from the Ashanti belt to the west by the Cape Coast Basin and from the Pan-African Dahomeyide belt to the east by the Suhum Basin (Fig. 2a: Agyei-Duodu et al., 2009).

The Suhum Basin separates the Kibi-Winneba belt into the northern Kibi and southern Winneba belts (Fig. 2a and b). To the west and east of the Suhum Basin are the Cape Coast Basin and Pan-African Dahomeyide belt, respectively, and to the north is the Voltaian Supergroup (Fig. 2a and b). Fig. 3 illustrates the lithological distribution and relationship of the Suhum-Akwadum area of the Suhum Basin. From Fig. 3, the Suhum-Akwadum area is underlain by (1). Amphibolite originates partially as a result of contact metamorphism (2). Biotite granitoid, which are mostly granodioritic in composition (2132 ± 4 Ma), described as "Tamnean" protoliths, are also affected by Eburnean Tectono-metamorphic overprinting. (3). K-feldspar-rich granitoids, mainly granite and monzonite (2088 ± 1 Ma), are locally leucogranitic. (4). Locally migmatitic biotite gneisses and minor biotite schists (metasedimentary rock), which may include garnet and/or amphibole, dated at 2187±1Ma and 2165 ± 9 Ma (Davis et al., 1994; Hirdes et al., 1996; Hirdes and Davis, 1998). (5). Pre-Mesozoic mafic dolerite dyke, inferred from aeromagnetic data. These are bounded by basalts and subvolcanic rocks interbedded with minor volcaniclastics of the Kibi belt and Biotite granitoid of the Cape Coast Basin to the east (Fig. 3). The rocks in the Suhum-Akwadum area have generally undergone up to greenschist facies regional metamorphism. However, the metasedimentary and mafic rocks near the granitoids display various degrees of contact metamorphism up to amphibole-hornfels facies (Agyei-Duodu et al., 2009). The rocks have been affected by low-grade metasomatic alterations involving silicification and widespread formation of secondary chlorite and sericite.

2. Materials and methods

Fig. 3 shows the various lithological units in the study area, with sampling points of amphibolite represented by red-filled triangles and those for the schists represented by filled blue squares. The short, dashed circles indicated the various areas where the schists (blue) and amphibolite (red) were observed. Sixteen fresh samples were prepared into thin sections, and their texture and mineralogy are studied using the Leica DM750P polarising microscope.

Ten amphibolite and six schist rock samples were selected for whole-rock geochemical analysis. The sample preparation followed standard procedures at the ALS laboratory outlet in Kumasi, Ghana. The crushed rock chips were reduced to a powder below 2 mm (<70 %). Later, the samples were split using a riffle splitter and pulverising through <75 μm (pulverised split to 85 %). Standard procedures were followed for Crushing QC and Pulverising QC tests at the ALS laboratory. The Inductively Coupled Plasma Atomic Emission Spectrometry (ICP-AES) method was used for the major element analysis at the ALS laboratory in Vancouver, following the standard procedure accredited to ISO/IEC 170252005 standards. The Inductively Coupled Plasma-Mass Spectrometry (ICP-MS) technique was used to analyse the trace elements. The results were corrected for spectral interference, and the necessary geochemical diagrams were plotted to aid data interpretation. Protocols for the analyses can be found in Nude et al. (2015). Precision is generally better than 2 %.

3. Results

3.1. Petrography

3.1.1. Amphibolite

The amphibolite occurs as elongated units, mostly in contact with the granitoids, with baked contact and chill margins in some places, and as large enclaves within the granitoids, as shown in Fig. 4a and b. The field mapping has revealed a greater occurrence of the amphibolite than reported previously (Fig. 3). They are generally dark green and medium to

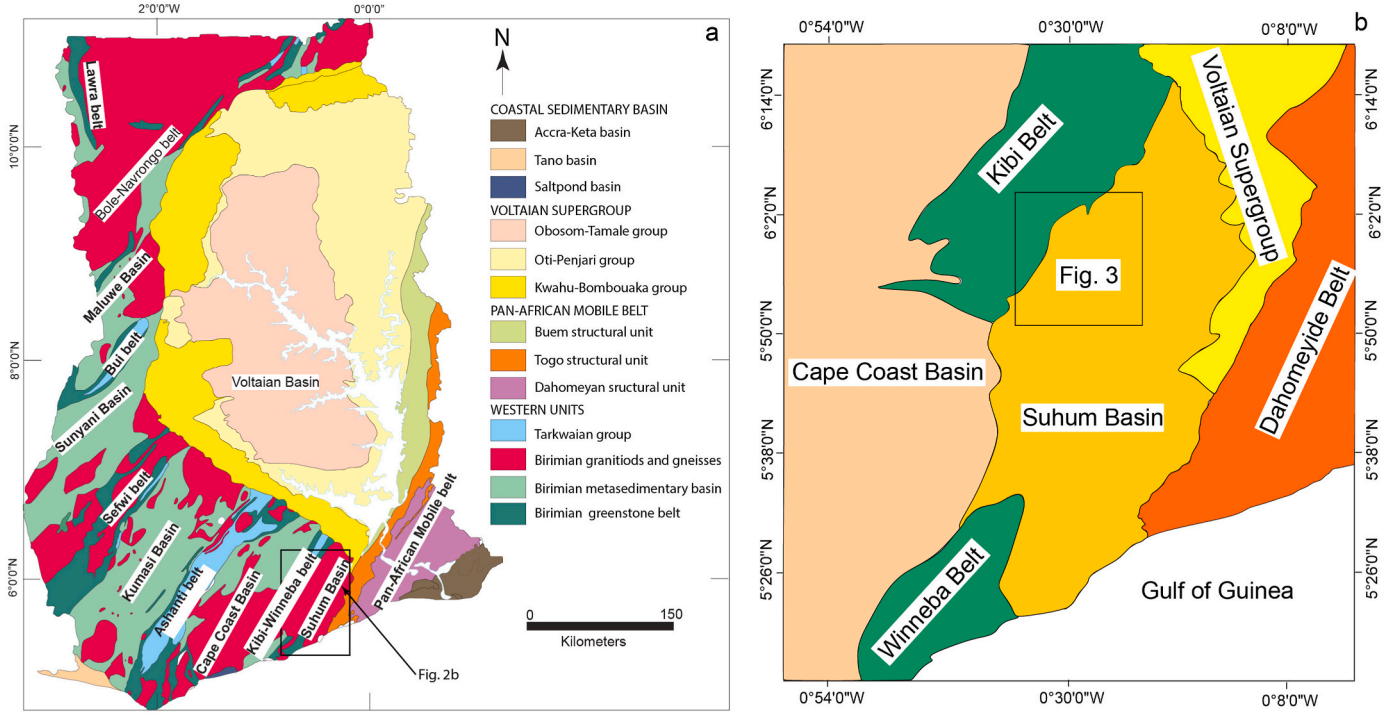

Fig. 2. (a) Geological map of Ghana showing the various greenstone belts and metasedimentary basins (after Agyei-Duodu et al., 2009), and (b) Geological map of the Kibi-Winneba belt (after Agyei-Duodu et al., 2009).

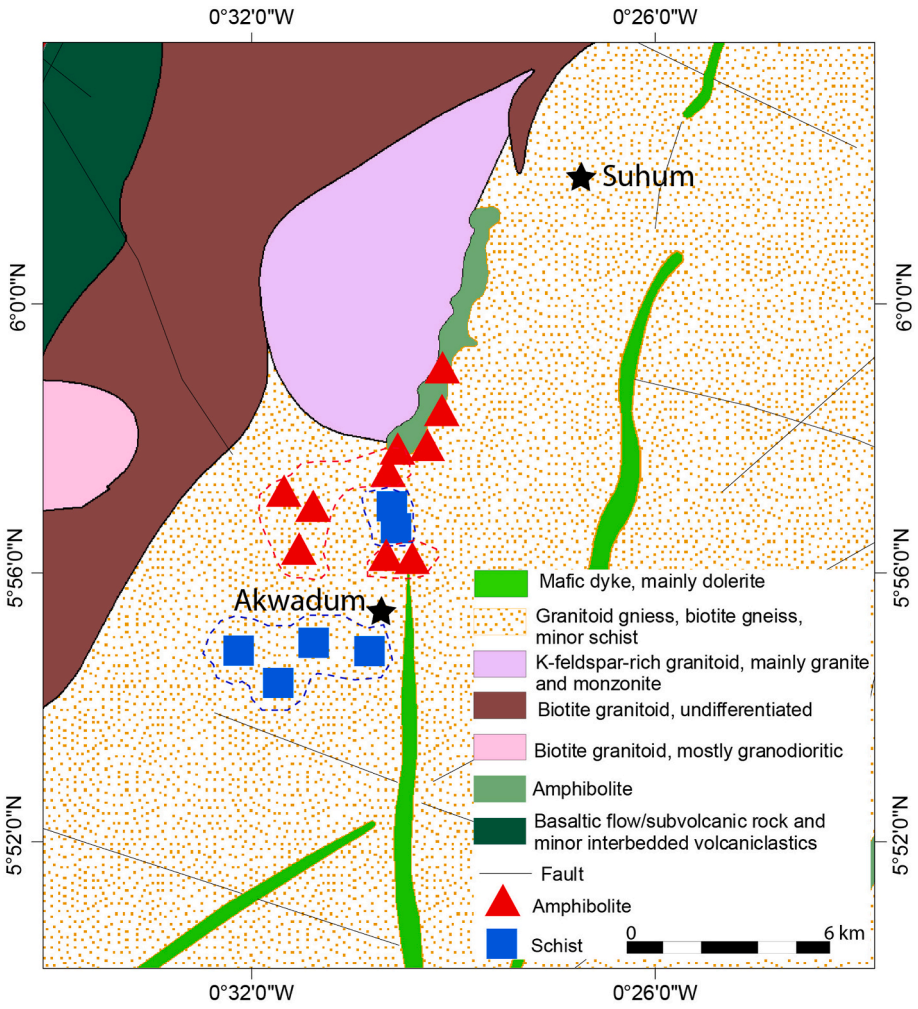

Fig. 3. Geological map of the study area. Note: the red triangle symbols represent sample locations for amphibolite, whereas the blue square symbols are for schist sample locations.

coarse-grained (Fig. 4a). The amphibolite is composed predominantly of amphibole (mainly hornblende, 20–85 %), plagioclase (10–12 %) and pyroxene (4–40 %) (Fig. 4b). The hornblende and pyroxene have undergone partial alteration into chlorite (5–35 %) and epidote (3–30 %), whereas the plagioclase is partially altered to sericite (6–15) and carbonate minerals (4 %). A trace amount of opaque minerals (<1 %) can be observed, mainly as alteration products of the ferromagnesian minerals. The estimated modal composition of amphibolite is presented in Table 1. Quartz (2–14 %) is also observed in some samples. In some samples, the mineral assemblage shows a somewhat preferred orientation.

3.2. Schists

The schists have been intruded by the granitoids, and even in some places, they occur as enclaves within the granitoids (Fig. 5a and b). Two types of schists were identified: hornblende-biotite schist and muscovite-biotite schist. They are generally fine to medium-grained and exhibit strong schistosity, defined by the preferred alignment of micas and hornblende (Fig. 5c–e). The hornblende-biotite schist contains 35–40 % biotite, 20–30 % hornblende, 15–25 % Quartz, and 10–15 % plagioclase (Table 2). The ferromagnesian minerals have significantly altered to chlorite and epidote (Fig. 5c). The muscovite-biotite schist contains 40–50 % quartz, 35–40 % biotite, 10–15 % plagioclase, and 5 % muscovite (Table 2).

3.3. Major and trace element geochemistry

The geochemical data for the 16 samples (10 amphibolite and 6 schists) are presented in Table 3.

3.3.1. Amphibolite

The amphibolite in the Suhum-Akwadum area of the Suhum Basin has a narrow range of SiO_2 contents, ranging from 47.3 to 50.2 wt %. They have moderate to high TiO_2 (0.90–2.29 wt %), MgO (3.93–9.90 wt %), and high Al_2O_3 (10.8–15.80 wt %), Fe_2O_3 (10.4–16.1 wt %) and CaO (9.89–14.90 wt %) contents. The high Fe_2O_3 content and moderate to high MgO content correspond to low to moderate Mg# (31–59). The LOI contents recorded for the amphibolite are very low (0.20–1.35 wt %; Table 3). The study area amphibolite has low to moderate Cr (100–640 ppm), Ni (32–339 ppm), Co (39–56 ppm), and Zr (60–203 ppm) contents. Their Ni, Ti, and Zr contents indicate that they are igneous amphibolite (Fig. 6a and b) (Winchester and Max, 1982). The study area amphibolite plot as sub-alkaline magma series and can be classified as subalkaline basalt, similar to the mafic volcanic and mafic intrusives of the Kibi belt (Fig. 6c and d; (Sakyi et al., 2018).

The amphibolite found in the Suhum-Akwadum area generally depicts a nearly flat REE pattern, which is similar to MORB on the Chondrite-normalised REE diagram, with no noticeable Eu anomalies ($Eu/Eu^* = 0.85–1.03$; Fig. 7a; Gale et al., 2013). However, two samples display a relative enriched (E-MORB/OIB) pattern (Fig. 7a). The La/Yb values of the amphibolite range from 1.30 to 2.63, except for three

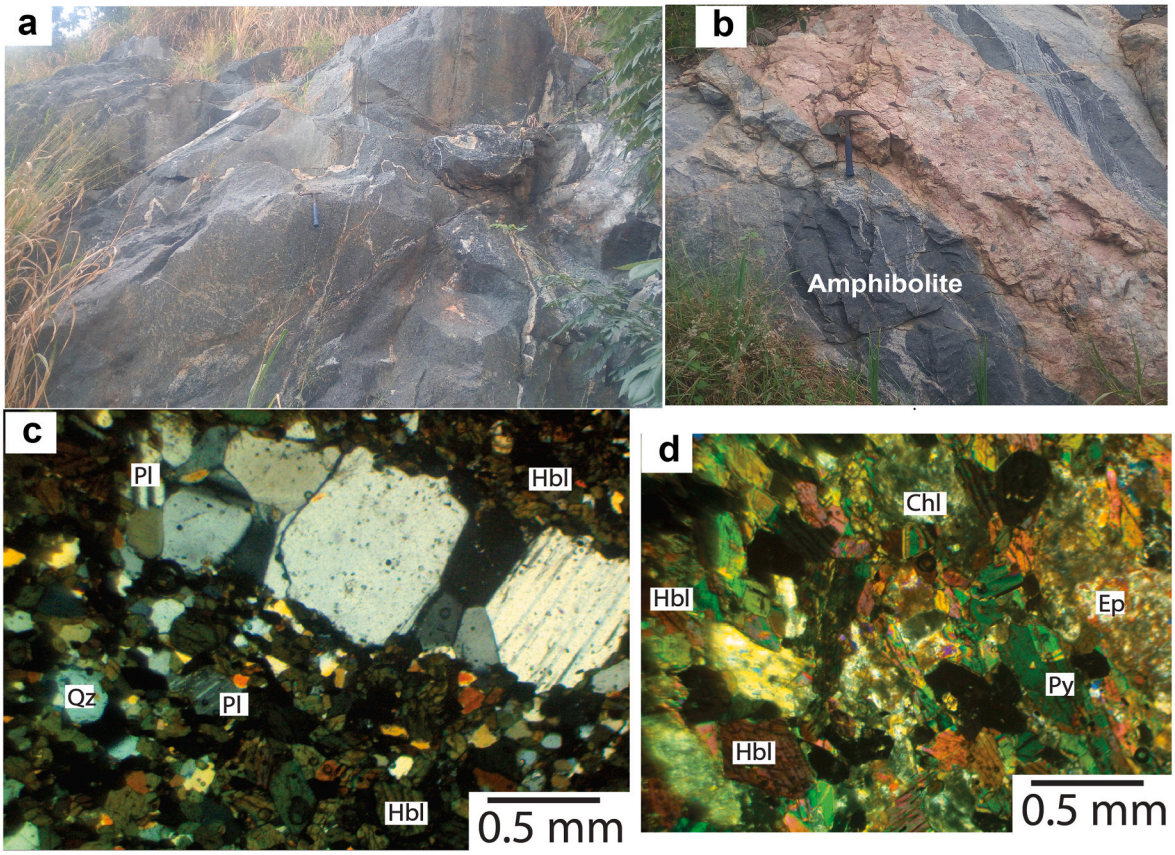

Fig. 4. (a) field photo of amphibolite, (b) large enclaves of amphibolite inclusions in the granitoid, (c) photomicrograph of the amphibolite showing hornblende-plagioclase microtexture and (d) photomicrograph of amphibolite showing significant alteration of the ferromagnesian minerals.

Table 1
The estimated modal composition of amphibolite.

	AS01A	AS09B	AS01B	AS05B	AS05A	AS05C	AS015A(18)	AS018A	GR014A	GR014B
Amphiboles	20	–	25	25	75	85	75	65	85	75
Feldspars	–	10	12	10	–	–	–	12	–	–
Pyroxenes	25	45	25	40	–	–	–	–	4	–
Quartz	–	2		–	8	8	–	14	5	5
Chlorites	10	35	25	20	–	–	5	–	–	5
Epidotes	30	8	3	–	–	–	10	9	–	–
Sericites	15	–	10	5	12	7	9	–	6	15
Carbonates	–	–		–	4	–	–	–	–	–
Opaque					<1	<1	<1	<1	<1	<1

samples that have LREE-enriched patterns and depleted HREE patterns, which correspond to high La/Yb values of 12.76–14.20 (Table 3). The REE pattern of the amphibolite is comparable to the mafic volcanic rocks of the Kibi belt (Sakyi et al., 2018). However, the amphibolite exhibits weaker REE fractionation than the mafic volcanic rocks of the Kibi belt (Fig. 7a). The multi-element normalised to primitive mantle diagram for the amphibolite of the Suhum-Akwadum area is characterised by Nb-Ta, P, and Ti negative peaks (Fig. 7b). Overall, the multi-element pattern for the amphibolite of the Suhum-Akwadum area is similar to the mafic volcanic rocks of the Kibi belt (Fig. 7b; Sakyi et al., 2018). This near-flat multi-element pattern is similar to rocks derived from MORB sources (Gale et al., 2013).

3.3.2. *Schists*

The schists from the Suhum-Akwadum area of the Suhum Basin exhibit significant variations in their major element compositions, characterised by a wide range of SiO_2 contents of (54.8–71.3 wt %), TiO_2 of (0.55–1.49 wt %) Fe_2O_3 of (4.88–14.95 wt %), MgO of (1.03–2.14 wt %), and CaO of (2.05–7.08 wt %). However, they have somewhat restricted Al_2O_3 (12.9–15.9 wt %), Na_2O (2.80–3.80 wt %), K_2O (1.02–2.26 wt %) and P_2O_5 (0.13–0.61 wt %) contents. On the SiO_2 vs TiO_2 diagram (Tarney, 1977), the schists from the Suhum-Akwadum area mainly plot in the sedimentary protolith field (Fig. 8a). The schists show major element composition similar to shales and wackes and metasedimentary rocks of the Birimian terrane (Fig. 8b; Asiedu et al., 2007, 2009, 2017, 2019; Manu et al., 2013; Sakyi et al., 2019).

The schists are characterised by enriched concentrations of the LREEs and depleted HREE contents with pronounced Eu anomalies (Eu/Eu* = 0.62–0.84) on the Chondrite-normalised REE diagram (Fig. 9a). This REE pattern is akin to Upper Continental Crust (UCC) and Post Archeean Australian Shale (PAAS) and falls within the field of Birimian metasedimentary rocks (Fig. 9a) (Rudnick, 2005; Mclennan, 2018; Sakyi et al., 2019). On the multi-element diagram normalised to UCC (Fig. 9b) (Rudnick, 2005), the schists from the study area display nearly flat LILE contents and enriched HFSE and REE contents, with negative peaks of Rb, K, Sr and Ti. Although the LILE contents of the schists of the

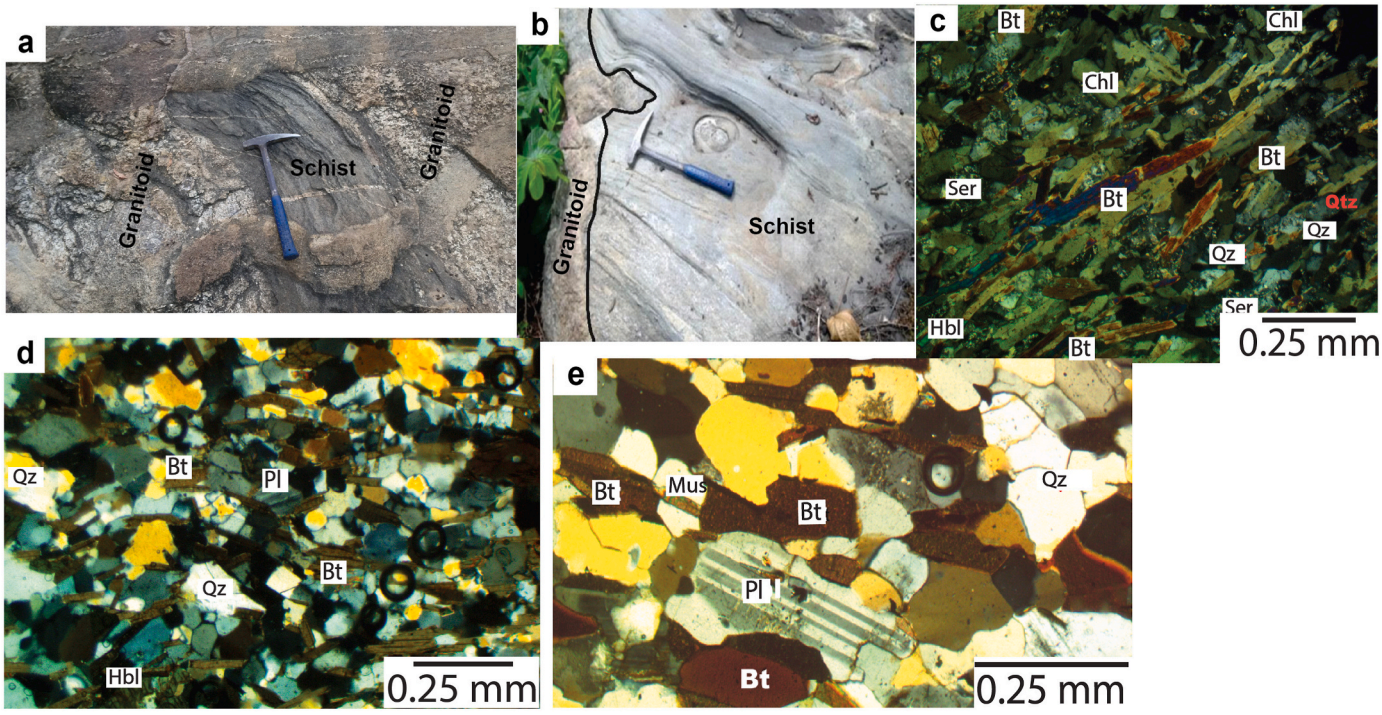

Fig. 5. (a) field photo of enclave of schist included in the granitoids, (b) field photo of schist in contact with granitoid, (c) photomicrograph of schist showing significant alteration of biotite and hornblende into chlorite and epidote, (d) hornblende-biotite schist with biotite-hornblende defining the schistosity and (e) muscovite-biotite defining schistosity in the muscovite-biotite schist.

Table 2
The estimated modal composition of schists.

	AS06A	AS06E	AS08.1A	AS08.1C	AS014A	AS014C
	Hornblende-biotite schist				Muscovite-biotite schist	
Hornblende	25	25	30	20	–	–
Feldspars	10	5	13	22	15	10
Biotites	35	35	40	35	40	35
Muscovites	–	–	–	–	5	5
Quartz	25	19	15	20	40	50
Chlorites	5	15	2	3	–	–
Sericites	–	–	–	–	–	–
Opaque Minerals	–	1	–	–	–	–

Suhum-Akwadum area are similar to UCC and PAAS, their HFSE and REE contents are slightly higher than UCC and PAAS (Fig. 9b) (Mclennan, 2018; Rudnick, 2005). The overall multi-element pattern of the schists is akin to the metasedimentary rocks of the Birimian (Fig. 9b; Asiedu et al., 2007, 2009, 2017, 2019; Manu et al., 2013; Sakyi et al., 2019).

4. Discussion

4.1. Petrogenesis of the Suhum-Akwadum area amphibolite

The amphibolite in the Suhum-Akwadum area experienced weak mineral alteration and high metamorphism, likely under amphibolite facies conditions. The presence of chlorite, epidote, sericite, and quartz may indicate retrograde metamorphism under greenschist facies. Low LOI contents (0.20–1.35 wt%) suggest minimal alteration and limited element mobility. Element mobility was assessed using Zr versus major and trace elements. Significant mobility was indicated by negative trends between Zr, K_2O, and Ba, whereas stable elements such as TiO_2, Na_2O, Th, Nb, Hf, La, and Y exhibited positive, coherent trends (Fig. 10). Plot of Zr/Hf and Y/Ho (Bau, 1996, Fig. 11) confirmed minimal alteration effects on HFS, REE, and some major elements, supporting their reliability for petrogenetic interpretations.

4.2. Magma source and evolution

Evolved magmas typically have low Ni, Cr and Mg# contents (Winter, 2001), which is characteristic of the Suhum-Akwadum area amphibolite (Table 3), which suggests that they are from evolved magma. The moderate to high TiO_2 contents, coupled with the nearly flat REE and multi-element patterns, suggest that these samples were derived from moderate to enriched mantle sources like E-MORB and OIB or were formed by different degrees of partial melting of the same source but at different depths (Sun and McDonough, 1989; Gale et al., 2013). The enriched LREE pattern relative to HREE exhibited by some samples may probably be due to variable degrees of partial melting at different depths or the melting of different sources (Gale et al., 2013; Hofmann, 2014). Higher Zr/Nb ratios (around 28) are characteristic of N-MORB, whereas lower Zr/Nb values of (5.8–6.4) are typical of rocks from E-MORB and OIB sources, respectively (Sun and McDonough, 1989; Gale et al., 2013). The amphibolite of the Suhum-Akwadum area have Zr/Nb ratios between 10 and 29, indicating a MORB-like source as the origin of the Suhum-Akwadum amphibolite. Peate et al. (1999) and Song et al. (2001) indicate that because the ratio of La/Nb varies between MORB-like sources (with La/Nb $>$ 1) and OIB-like sources (with La/Nb $<$ 1), it can be used to determine the source of magma. The La/Nb values for the amphibolite are in the range of 1.0–8.2, suggesting the melting of a MORB-like magma source, although, source enrichment of an enriched component or sediment recycling cannot be ruled out. The wide variations of the Zr/Nb and La/Nb values for the amphibolite, coupled with their REE patterns, imply they were probably derived from variable degrees of partial melting of MORB-like sources at different depths or two distinct sources.

Table 3
Geochemical data for the amphibolite and schists.

Amphibolites										
Sample	AS01A	AS09B	AS01B	AS05B	AS05A	AS05C	AS015A(18)	AS015B(18)	GR014A	GR014B
wt%										
SiO2	48.3	50	50.2	47.3	47.2	48.7	48.8	48	48.9	47.3
TiO2	1.11	1.37	0.91	1.26	1.26	1.23	2.29	2.29	0.9	0.97
Al2O3	13.75	13.1	14.1	11.1	11.25	10.8	14.65	14.4	14.15	15.8
Fe2O3	13.3	12.5	13	12.25	12.25	12.1	15.9	16.1	10.4	11.85
MnO	0.23	0.18	0.22	0.19	0.19	0.19	0.25	0.25	0.21	0.2
MgO	6.33	5.94	5.99	9.6	9.6	9.9	3.93	4.02	5.84	5.85
CaO	11.3	11.45	11.15	13	12.95	13.05	9.89	9.96	14.9	13.35
Na2O	2.89	2.78	1.6	1.99	1.94	1.99	2.76	2.69	1.32	1.9
K2O	0.66	0.51	0.99	0.49	0.43	0.47	0.49	0.49	0.56	0.53
P2O5	0.13	0.11	0.11	0.46	0.45	0.44	0.31	0.31	0.09	0.09
LOI	1.33	0.55	0.89	1.16	0.86	1.02	0.26	0.2	1.35	1.23
Total	99.39	98.54	99.25	98.98	98.56	100.07	99.6	98.77	98.7	99.13
ppm										
Co	55	43	48	54	56	54	41	39	40	46
Ni	77	67	109	311	305	339	32	33	73	73
Pb	2	2	4	6	2	5	6	6	4	3
Sc	42	35	39	41	41	42	36	35	32	35
Zn	106	91	96	109	110	105	138	135	79	83
Ba	170	106	164.5	232	289	289	141.5	135.5	244	145.5
Ce	18.4	17.6	17.1	104.5	98.8	104.5	41.4	39.8	14.8	12.1
Cr	140	100	340	590	560	640	120	110	210	180
Cs	0.7	0.16	2	0.26	0.21	0.39	0.21	0.16	4.74	2.82
Dy	4.48	5.49	3.86	6.11	5.73	6.06	9.47	9.06	4.14	4.15
Er	2.81	3.2	2.37	2.49	2.6	2.73	5.91	5.5	2.74	2.52
Eu	1.21	1.55	0.84	3.45	3.32	3.37	2.25	2.13	1.17	1.02
Gd	4.09	5	3.68	9.72	9.21	10.1	8.6	8.35	4.11	3.49
Hf	1.9	2.6	1.8	3.5	3.8	3.8	5.5	5.1	2.2	1.8
Ho	0.96	1.12	0.8	1.08	1.04	1.08	2	1.93	0.93	0.85
La	7.8	10.1	7.4	41.1	39	40.9	18.1	17.6	6.5	4.7
Lu	0.38	0.4	0.32	0.3	0.29	0.32	0.79	0.8	0.42	0.38
Nb	3.4	4	3.3	5	5.7	5.6	12.1	11.6	6.5	2.1
Nd	12.3	16.1	10.7	64.5	61.1	65.2	26.9	25.8	9.9	8.7
Pr	2.54	3.27	2.29	14.5	13.8	14.45	5.83	5.65	2.06	1.75
Rb	23.3	7.3	25.6	8	4.1	7.1	5.7	5.5	27.6	17.3
Sm	3.42	4.36	2.89	12.85	11.7	12.75	7.1	6.93	3.07	2.59
Sr	237	296	228	632	631	610	272	251	310	232
Ta	0.1	0.2	0.1	0.2	0.2	0.2	0.7	0.7	1.3	0.1
Tb	0.71	0.87	0.62	1.17	1.15	1.17	1.52	1.33	0.68	0.63
Th	0.64	0.42	0.83	1.65	1.75	2.31	2.07	1.95	0.63	0.49
Tm	0.41	0.43	0.36	0.37	0.33	0.34	0.79	0.8	0.39	0.38
U	0.19	0.16	0.19	0.49	0.55	0.67	0.56	0.54	1.45	0.2
V	325	383	274	235	222	240	279	262	250	276
Y	24.4	29.1	21.3	27.4	25.8	27.8	52.4	50.9	24.4	23
Yb	2.58	2.68	2.31	2.16	1.92	2.24	5.37	5.21	2.74	2.52
Zr	69	93	70	134	146	146	203	199	66	60

Schists						
Sample	AS06A	AS06E	AS08.1A	AS08.1C	AS014A	AS014C
wt%		Hornblende-biotite			Muscovite-biotite	
SiO2	55.1	54.8	62.2	61.8	67.7	71.3
TiO2	1.49	1.46	0.91	0.86	0.55	0.55
Al2O3	13.75	13.75	12.9	13.25	15.9	13.7
Fe2O3	15	14.95	11.2	10.75	4.98	4.88
MnO	0.24	0.25	0.17	0.2	0.07	0.06
MgO	2.14	2.02	1.31	1.03	2.04	1.44
CaO	6.61	7.08	4.34	5.09	2.05	2.19
Na2O	2.8	2.93	2.87	3	3.67	3.8
K2O	1.38	1.02	2.26	1.92	2.8	1.87
P2O5	0.61	0.59	0.3	0.25	0.24	0.13
LOI	0.35	0.26	0.33	0.26	1.23	0.62
Total	99.53	99.18	98.88	98.51	101.37	100.65
ppm						
Co	19	19	9	7	13	10
Ni	9	6	4	2	18	21
Pb	12	10	8	12	15	11
Sc	29	28	20	19	9	9
Zn	190	182	199	211	74	82
Ba	402	395	697	706	870	617
Ce	120	116	151	165.5	81.4	68.6
Cr	30	20	20	20	50	70
Cs	3.4	1.83	10.15	5.83	19.75	16.9

(*continued on next page*)

Table 3 (*continued*)

Schists						
Sample	AS06A	AS06E	AS08.1A	AS08.1C	AS014A	AS014C
wt%		Hornblende-biotite			Muscovite-biotite	
Dy	13.8	13.4	15.5	17.6	3.57	2.59
Er	7.86	7.97	9.56	10.7	1.84	1.3
Eu	3.7	3.54	3.51	3.82	1.15	1.06
Gd	14.55	13.85	15.4	16.9	5.02	3.29
Hf	9.6	9.3	13.9	15.5	4.6	4.9
Ho	2.67	2.76	3.27	3.73	0.7	0.47
La	58.3	52.9	70.3	76.6	40.8	28.7
Lu	1.07	1.16	1.35	1.6	0.23	0.16
Nb	31.8	32.3	37.1	42.5	11.9	8.2
Nd	66.6	60.5	74.1	80.8	34.5	25.8
Pr	15.9	14.45	18.4	19.8	9.12	6.69
Rb	52.1	30.6	92.7	62.5	112.5	119.5
Sm	13.8	13.4	15.8	17	6.22	4.45
Sr	225	250	212	251	346	422
Ta	2.1	2	2.3	2.6	0.6	0.6
Tb	2.22	2.18	2.45	2.76	0.67	0.47
Th	6.67	6.56	9.5	10.7	7.09	5.55
Tm	1.11	1.16	1.32	1.59	0.27	0.16
U	1.72	1.75	2.54	2.83	2.26	1.9
V	48	45	26	24	91	63
Y	71.6	74.2	88.2	99	18.8	11.8
Yb	7.09	7.41	9.1	10.65	1.86	1.04
Zr	379	386	575	649	174	182

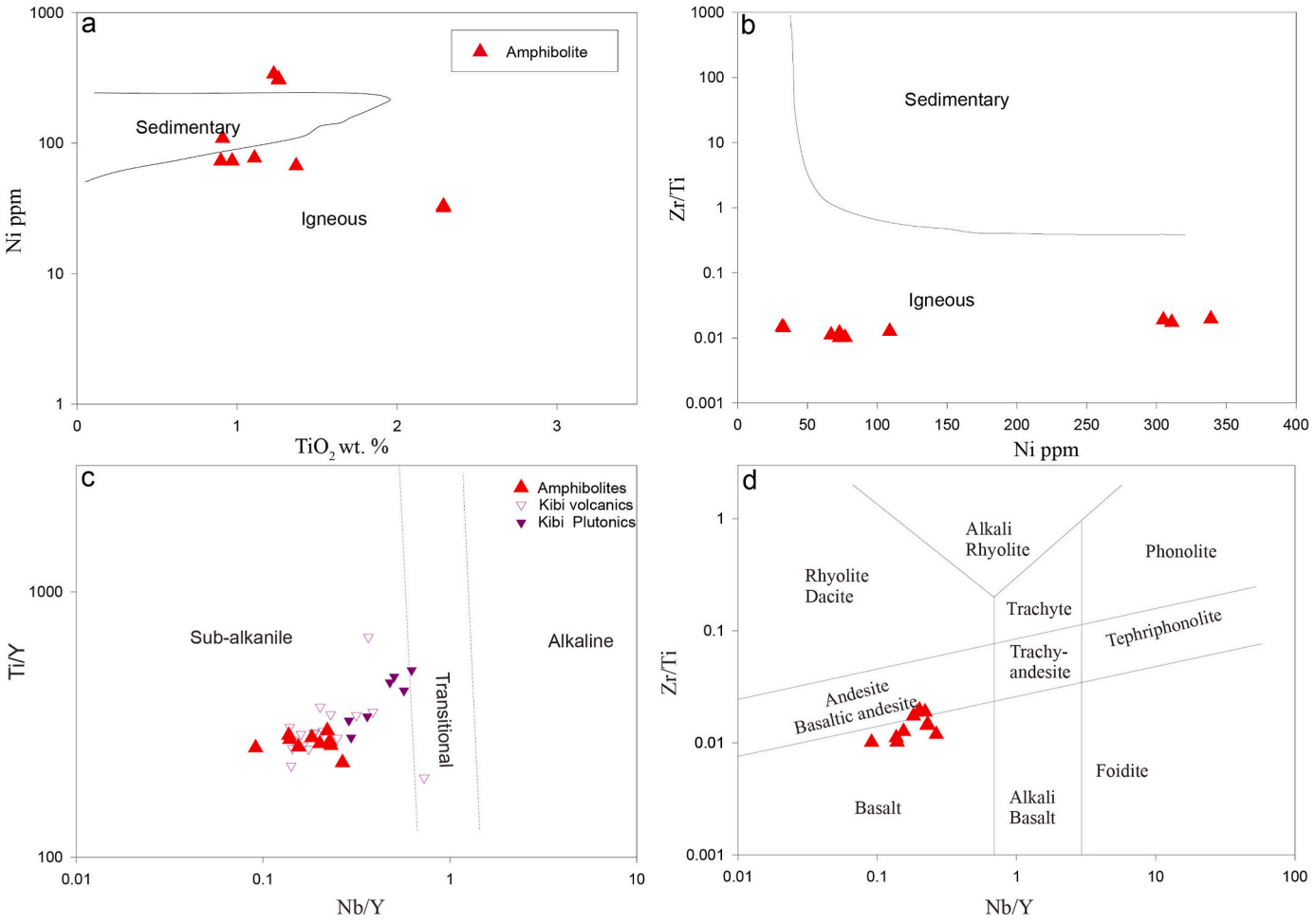

Fig. 6. Amphibolite classifications (after Winchester and Max, 1982) (a) TiO_2 vs Ni, (b) Ni vs Zr/Ti, (c) Nb/Y vs Ti/Y (after Pearce and Wyman, 1996), and (d) Nb/Y vs Zr/Ti (after Pearce and Cann, 1973).

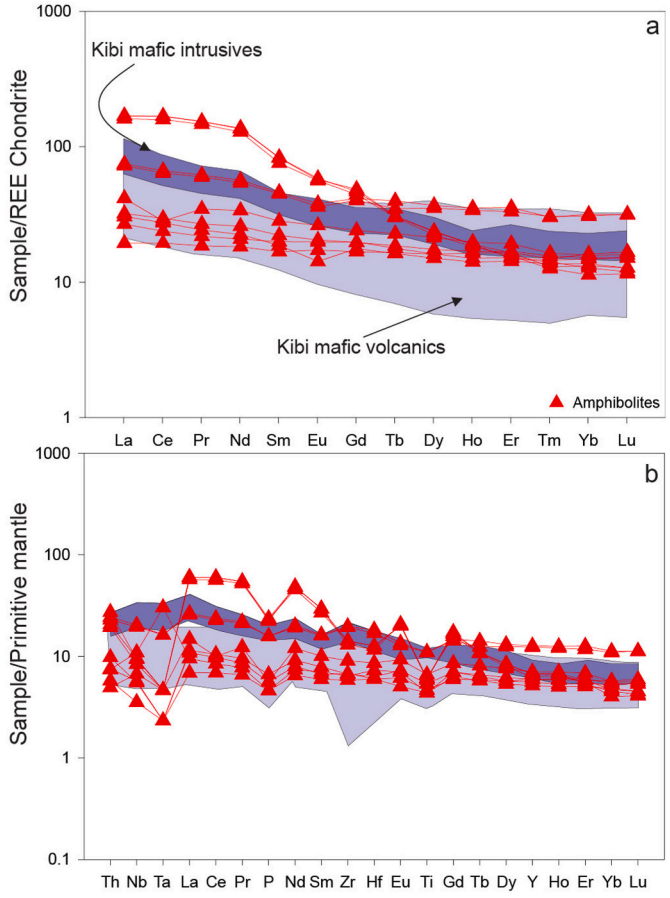

Fig. 7. (a) Chondrite-normalised REE and (b) Primitive mantle-normalised diagrams for the amphibolite. The amphibolite data is compared to the data from the Kibi belt (Sakyi et al., 2018).

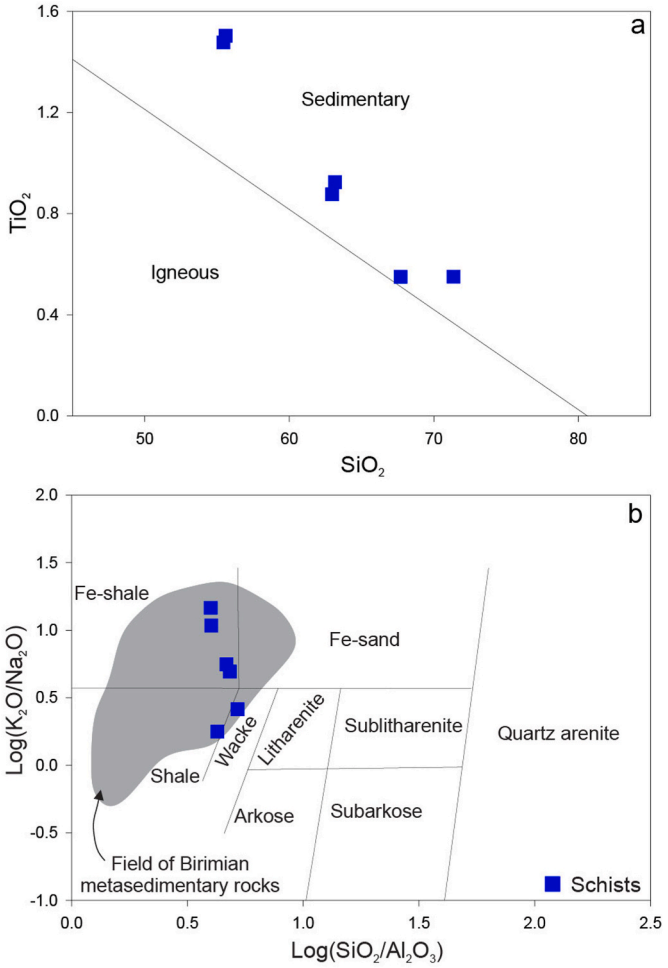

Fig. 8. Classification diagrams for the schists (a) Plot of SiO_2 vs. TiO_2 (Tarney, 1977), and (b) Log (SiO_2/Al_2O_3) vs Log (Fe_2O_3/K_2O) (fields after, Herron, 1988). Data for the field of Birimian metasedimentary rocks is from (Asiedu et al., 2007, 2009, 2017, 2019; Manu et al., 2013; Sakyi et al., 2019).

4.3. Melting source and depth

Several factors, such as the extent of partial melting, the presence of spinel or garnet in the mantle source, and the overall geochemical composition of the source, influence the composition of mantle-derived magmas (McDonough and Rudnick, 1998; Yaxley, 2000; Xu et al., 2005; Lai et al., 2012; Manikyamba et al., 2015). REEs play a crucial role in determining the melting conditions in the mantle (McDonough and Rudnick, 1998; Manikyamba et al., 2015). The HREEs, especially Yb, are compatible, whereas LREEs like La and MREEs such as Sm and Gd are incompatible in garnet (Blundy and Wood, 1994; Van Westrenen et al., 2001). This means Yb has a high garnet/melt partition coefficient relative to La, Sm, and Gd (Blundy and Wood, 1994; Van Westrenen et al., 2001). When a garnet lherzolite undergoes partial melting, the La/Yb and Sm/Yb ratios are strongly fractionated, whereas these ratios, especially the Sm/Yb ratios, remain relatively unchanged during partial melting in the spinel lherzolite stability field, although this depends on the degree of partial melting (Yaxley, 2000; Xu et al., 2005; Lai et al., 2012). On the (La/Yb)n vs (Sm/Yb)n diagram, the amphibolite of the Suhum-Akwadum area mostly plot between N-MORB and E-MORB, similar to the Kibi mafic volcanic rocks; however, three samples plot above OIB (Fig. 12a). This geochemical feature may indicate variable degrees of partial melting at different depths or derivation from two distinct sources. Similarly, on the Dy/Yb vs La/Yb plot, most of the amphibolite samples fall within the field of spinel-lherzolite stability, with three samples plotting in the garnet-lherzolite stability field (Fig. 12b), corroborating variable degrees of partial melting at different depths or derivation from two distinct sources. Thus, the amphibolites of the Suhum-Akwadum area were produced by different degrees of partial melting of or sourced from mantle source between spinel and garnet lherzolite stability fields, probably at depths 80 and 150 km (White and McKenzie, 1995; Reichow et al., 2005).

4.4. Influence of crustal contamination

On the primitive mantle-normalised diagram (Fig. 7b), the Suhum-Akwadum amphibolite depicts negative Nb, Ta and Ti peaks, which are typical of subduction-related rocks or rocks affected by continental crust contamination (Pearce and Peate, 1995; Elburg, 2010; Pearce, 2014). Th is generally higher in subduction zone-related fluids and continental crust materials than Nb and Yb. Consequently, Th/Yb in rocks influenced by subduction-zone-related fluid or continental crust material will be higher than Nb/Yb (Pearce and Peate, 1995). Such contaminated rocks will typically plot away from the mantle array towards elevated Th/Yb on the Th/Yb vs Nb/Yb diagram (Pearce and Peate, 1995; Hofmann, 1988; Manikyamba et al., 2020). Given that, the amphibolite from the Suhum-Akwadum plot within the mantle array, which may suggest insignificant contamination by subduction zone-related fluid or continental crustal contamination (Fig. 13a). However, mafic volcanic and intrusive rocks of the Kibi belt show evidence of magma-crust interaction during their evolution as they plot mostly away from the mantle array (Fig. 13a). Three samples, on the other hand, plot away from the mantle array, which may indicate source enrichment "metasomatism" by subduction zone component or

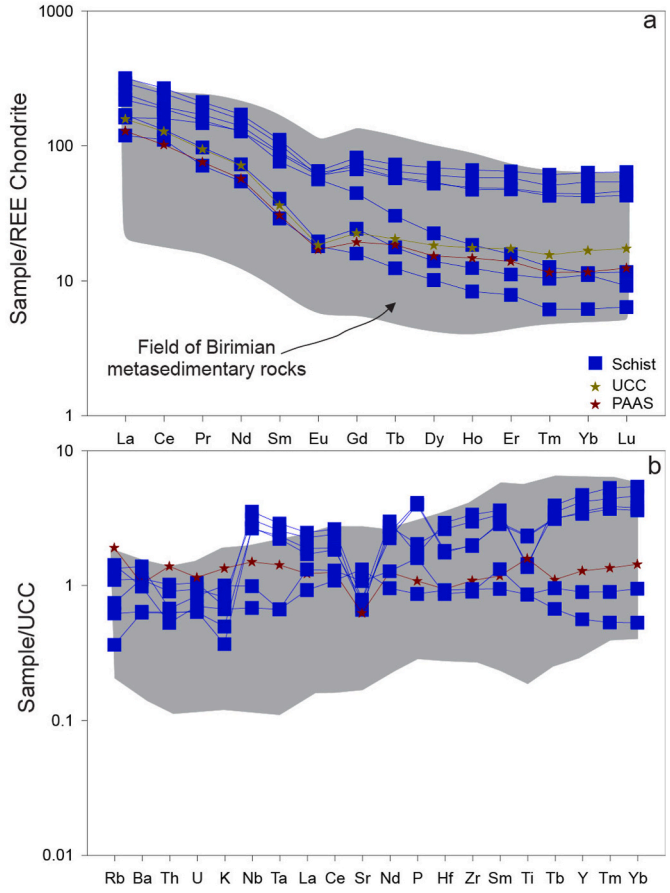

Fig. 9. (a) Chondrite normalised REE plot and (b) multi-element plot normalised to UCC for the schists. Data for the field of Birimian metasedimentary rocks is from (Asiedu et al., 2007, 2009, 2017, 2019; Manu et al., 2013; Sakyi et al., 2019).

sediment. All the amphibolite samples except two samples plot within the field defined by arc rocks or rocks influenced by continental contamination on the Nb/Th vs La/Nb diagram (Fig. 13b). This is similar to mafic volcanic and intrusive rocks from the Kibi blet. Continental crust contamination is expected to enrich the LILEs relative to HFS, which is not the case for most of the Suhum-Akwadum amphibolite (Fig. 7b). Thus, the geochemical features of the amphibolite might have experienced insignificant or very minimal continental crust contamination.

4.5. Depositional setting of the schists

The schists in the Suhum-Akwadum area, characterised by mica, quartz, and amphibole, suggest metamorphism under greenschist to lower amphibolite facies. Weak alterations such as sericitisation and chloritisation are observed. Low LOI, positive geochemical trends (Fig. 10), and position in the CHARAC field (Fig. 11) imply these elements remain immobile, validating their use in provenance and tectonic setting studies.

4.6. Paleoweathering conditions

The Chemical Index of Alteration (CIA = $Al_2O_3/(Al_2O_3 + CaO^* + Na_2O + K_2O)]^*100$) measures weathering of source rocks, indicating how primary minerals like feldspars have transformed into aluminous clays depleted in Ca, Na, and K (Nesbitt and Young, 1982). According to Roddaz et al. (2012) unaltered feldspars have a CIA of 50, similar to unaltered upper crustal rocks. In the Suhum-Akwadum area, the schists CIA values range from 47 to 56 (Table 3), close to 50, suggesting little to no weathering. K-metasomatism can lower CIA, so the Chemical Index of Weathering (CIW) was introduced (Harnois, 1988); higher CIW than CIA indicates more weathering and possibly K-metasomatism. In the Suhum-Akwadum area, CIW values of 50–67 (Table 3) show minimal weathering. The A-CN-K diagram confirms mostly no to incipient weathering, with most samples plotting below or on the' feldspar join" line (Fig. 14a).

McLennan and Taylor (1991) indicated that Th/U ratios reveal weathering conditions at the source of siliciclastic rocks. U is concentrated during sedimentation in reducing environments, resulting in lower Th/U ratios. Th/U ratios above 3 typically indicate weathering effects. The Th/U ratio also infers provenance, as ratios less than 3 suggest a passive margin source. McLennan et al. (1993) found that sediments from active margins have Th/U ratios of 1–6 and low Th concentrations. In contrast, the studied schists from the Suhum-Akwadum area have Th/U ratios of 2.92–3.88 and Th values of 6.56–10.70 ppm. Their weathering trend indicates an increasing weathering intensity, aligning with sources in and above depleted mantle arc fields, as shown in Fig. 14b. Low LOI, CIA, CIW, Th/U, and minimal mineral replacement suggest the schists experienced little to no source area weathering.

4.7. Sediment maturity, recycling, and source rock composition

The maturity of the Suhum-Akwadum schists was determined by calculating and evaluating the SiO_2/Al_2O_3 and Na_2O/K_2O ratios. Typically, mature siliciclastic sedimentary rocks have high SiO_2/Al_2O_3 ratios (>10) and low Na_2O/K_2O ratios (<1) (Cullers, 1994; Armstrong-Altrin et al., 2015; Hadji et al., 2024). The schists from the Suhum-Akwadum area exhibit low SiO_2/Al_2O_3 (3.99–5.20) and high Na_2O/K_2O values (1.27–2.87). These values suggest that the schists are composed of sediments that range from immature to moderately mature. The high Na_2O/K_2O values in the schists could be due to the presence of plagioclase feldspars, as observed from the petrographic investigation. The La/Sc ratio can be used to evaluate sediment maturity. The schists have low to moderate La/Sc values between 1.89 and 4.53, signifying immature to moderately mature sediments. Sedimentary rocks with mature sediments show a low (<1) index of compositional variability (ICV= $(Fe_2O_3 + K_2O + Na_2O + CaO + MgO + MnO + TiO_2)/Al_2O_3$), whereas first-cycled immature sediments show high (>1) ICV values. The Suhum-Akwadum schists have ICV values of 1.38–2.86, indicating compositional immaturity. In first-cycle sediments, Th/Sc ratios show an overall positive correlation with Zr/Sc, depending on the nature of the source rock. In contrast, Zr/Sc ratios in mature or recycled sediments display considerable variation with little accompanying change in Th/Sc (McLennan et al., 1993). A plot of the Th/Sc versus Zr/Sc (Fig. 15a) shows most of the analysed schist samples exhibiting a positive correlation within the mantle compositional fields with low Th/Sc values. This reflects the dominant input of rock materials from the mantle region having varying mineral or elemental compositions, with insignificant recycling. The mineralogical compositions, various ratios and plots have been utilised to determine the source rocks of the schists. The high percentage of amphibole (20–30 %) and biotite (35–45 %) in some of the schists may indicate they originated from mafic or intermediate source rocks. However, some samples have quartz between 15 and 50 %, feldspar between 10 and 22, and muscovite around 5 %, which may indicate felsic to intermediate source rocks. The concentrations of major and trace elements in siliciclastic sedimentary rocks are crucial in determining the composition of their source rock. Because mafic rocks have higher TiO_2 and lower Al_2O_3 concentrations compared to felsic rocks, the Al_2O_3/TiO_2 ratio can be used to assess the composition of the source rock of siliciclastic sedimentary rocks (Hayashi et al., 1997; Nagarajan et al., 2007). Typically, mafic rocks tend to have the lowest Al_2O_3/TiO_2 ratio of 3, followed by intermediate rocks with an Al_2O_3/TiO_2 ratio of 8 with the highest values of 21, recorded for felsic igneous

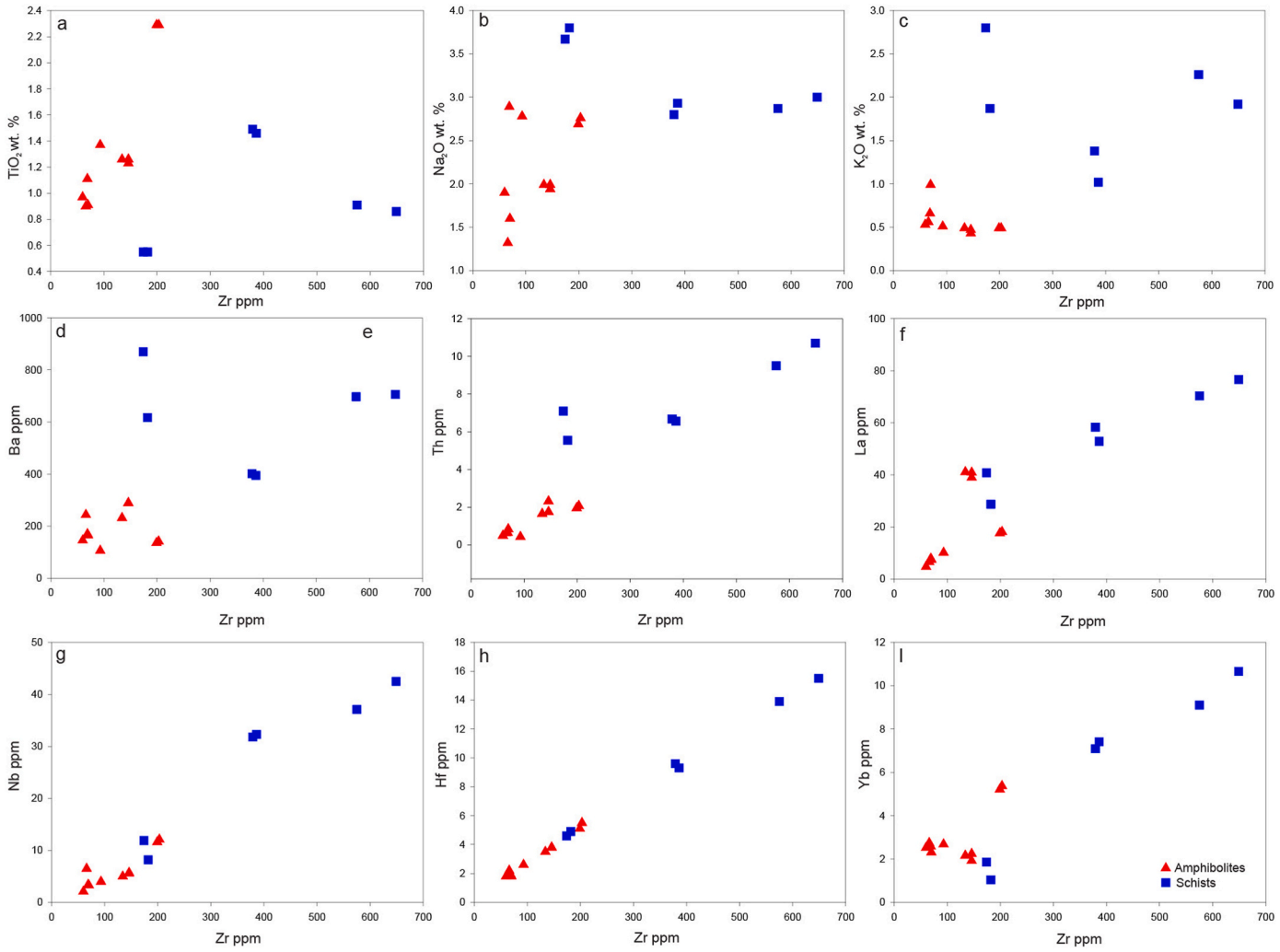

Fig. 10. Zr vs selected major and trace elements to assess elemental mobility of the amphibolites and schists.

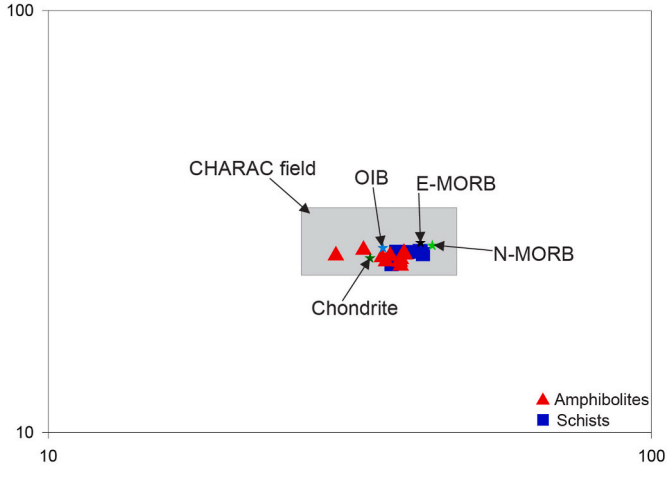

Fig. 11. Zr/Hf vs Y/Ho to assess the mobility of the trace elements after (Bau, 1996).

rocks (Hayashi et al., 1997). The schists of the Suhum-Akwadum area have moderate to high values of Al_2O_3/TiO_2 between 9 and 27, suggesting an intermediate to felsic source rock composition.

Generally, the REE patterns show little variation when sediments are sourced from a single source. On the other hand, significant variations in REE patterns are recorded when sediments come from multiple, diverse origins (Nance and Taylor, 1977; Taylor and McLennan, 1985; Cullers, 1995). In the case of the schists from the Suhum-Akwadum area, the REE patterns display slight variations (Fig. 9). This slight variation in REE patterns suggests diverse sediment sources, indicating that these rocks have variable provenances. Sc and Th often tend to be transferred easily from source to sediment without significant change in concentrations. Hence, Th/Sc ratios reflect bulk source compositions (Taylor and McLennan, 1985; McLennan and Taylor, 1991). On the Th/Sc versus Zr/Sc diagram (Fig. 15a), the schists were sourced from intermediate to felsic source rock as they plot between the compositions of andesite and TTG, similar to metasedimentary rocks from the Birimian terrane. Similarly, the La/Sc versus Co/Th plot also indicates an intermediate to felsic source rocks as the source rock composition for the Suhum-Akwadum area schists (Fig. 15b). The ratios of Cr/Th, Eu/Eu*, La/Co, $(La/Lu)_N$, La/Sc, Th/Sc, and Th/Co can provide valuable information about the composition of the source rock (Cullers, 1994, 2002; Cullers et al., 1988). From Table 4, the elemental ratios suggest that the sediments for the schists from the Suhum-Akwadum area were derived from intermediate and felsic source rocks. However, the high hornblende content in the hornblende-biotite schist could point to some mafic contribution. The Rhyacian Birimian terrane could be the probable source of sediments for the schists, as they comprise basaltic, basaltic andesitic and granitoid rocks.

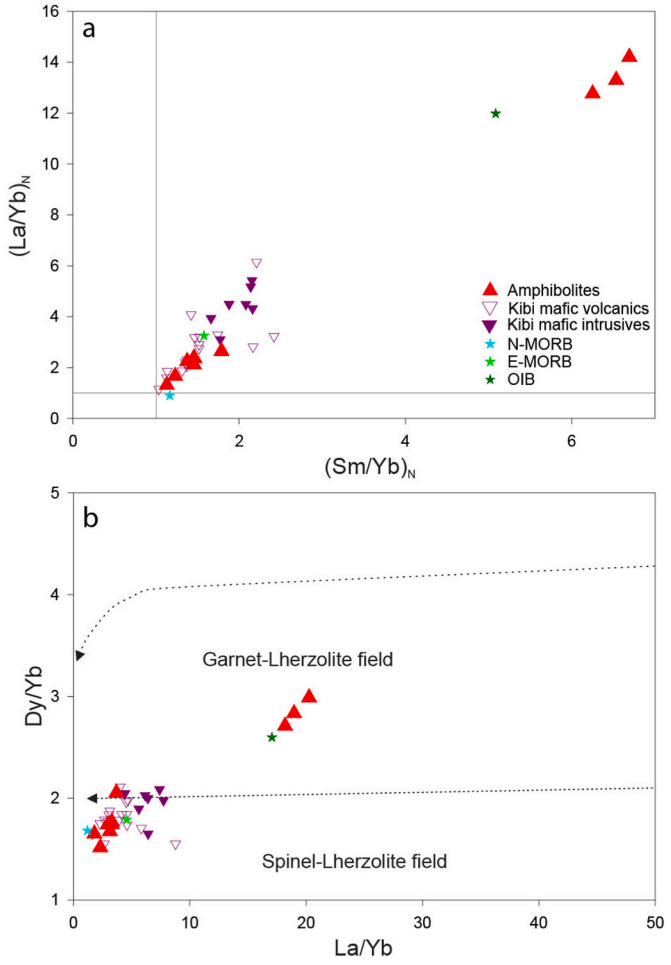

Fig. 12. (a) $(La/Yb)_N$ vs $(Sm/Yb)_N$ and (b) Dy/Yb vs La/Yb (after Jung et al., 2006) plots for the amphibolite. Kibi data is from Sakyi et al. (2018), whereas N-MORB and E-MORB values are from Gale et al. (2013) and OIB values from Sun and McDonough (1989).

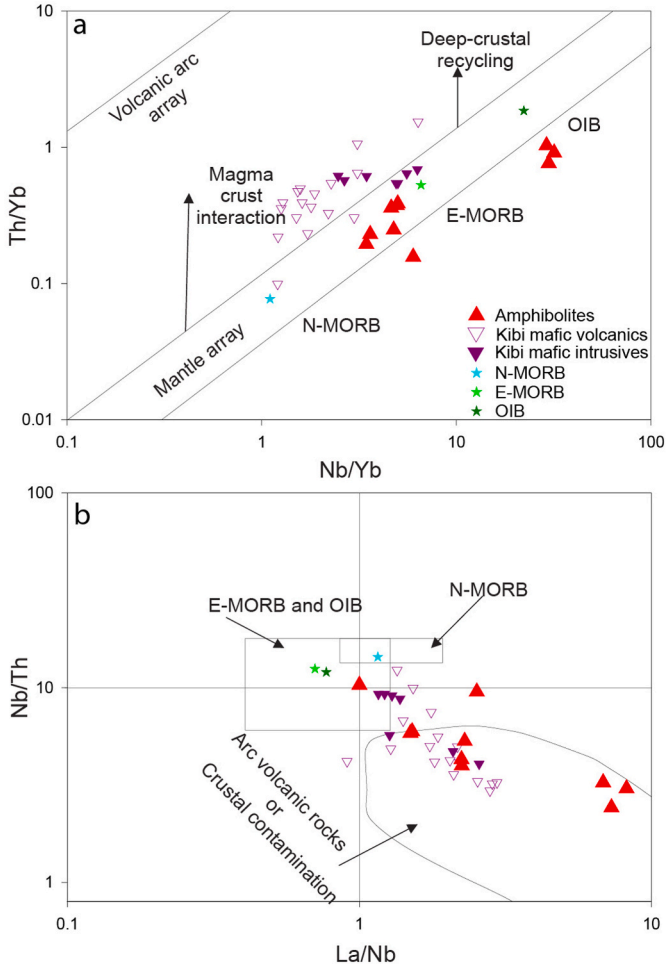

Fig. 13. a) Nb/Yb vs Th/Yb (after Pearce 2008) and (b) La/Nb vs Nb/Th plot (after Yang et al., 2019) for the amphibolite. Kibi data is from Sakyi et al. (2018), whereas N-MORB and E-MORB values are from Gale et al. (2013) and OIB values from Sun and McDonough (1989).

4.8. Provenance

McLennan et al. (1993, 1995) described five major provenance types based on geochemistry, the characteristics of which are summarised in Table 5. These provenance types are i) Old Upper Continental Crust, ii) Recycled Sedimentary Rock, iii) Young Undifferentiated Volcanic Arc, iv) Young Differentiated Volcanic Arc, and v) Exotic component. From this study, the majority of the results obtained suggest that the sources of the schists from the Suhum-Akwadum area are typical of Young Undifferentiated Arc terranes. The evidence leading to this deduction are:

1. Unevolved major and trace element compositions (e.g., low SiO_2/Al_2O_3, low CIA, Th/Sc, Zr/Sc ratios) in Table 5,
2. Variations of major and trace element compositions in Table 3, and low negative Eu anomalies,
3. Low REE abundances and variable but less LREE enrichment than those of Post-Archean Australian Sedimentary rock (PAAS).

The term "Young" refers to the age difference between the provenance terrane and the Birimian metasedimentary rocks. The available age data for the metasedimentary rocks indicate that their formation is contemporaneous with the Rhycian Birmian granitoid-greenstone belts (Leube et al., 1990). This implies that the metasedimentary rocks were derived from an arc crust that was not significantly modified by intracrustal differentiations. Asiedu et al. (2017) and Sedziafa et al. (2025) have observed similar provenance types from their studies on the metasedimentary rocks from the Kumasi Basin and Ashanti Belt.

4.9. Tectonic settings

Geochemical signatures such as Ti, Nb, and Ta enrichments are typical features of rocks from MORB or OIB environments (Sun and McDonough, 1989; Gale et al., 2013). On the other hand, subduction-related magmas are characterised by enrichment in Ba and Th and depletion in Nb, Ti, and Ta (Elburg, 2010; Fitton et al., 1988; Saunders et al., 1988). Therefore, the negative Ti, Nb, and Ta peaks observed in the amphibolite from the Suhum-Akwadum area (Fig. 7b) may suggest that they are derived from subduction-related magmas. Their enriched LILE and flat HFSE patterns are similar to those of rocks from a subduction zone setting (Elburg, 2010). The amphibolite plots on the island arc basalt and MORB field on the Zr vs TiO_2 diagram (Fig. 16a). Again, on the Zr-Y*3-Ti/100 diagram, the Suhum-Akwadum amphibolite plots in the field of MORB, island and calc-alkaline basalts (Fig. 16b). The ratio of Nb/Th have been useful in distinguishing rocks from arc and non-arc settings (Fitton et al., 1988). Typically, rocks derived from arc setting have low Nb/Th (<7.5) values (Fitton et al., 1988; Jenner et al., 1991; Gill, 2012). The Nb/Th ratios for the Suhum-Akwadum amphibolite are 2.4–10.3. The two samples with high Nb/Th values > 7.5 show they are different from arc-related rocks. Therefore, the amphibolite from the study area were probably derived

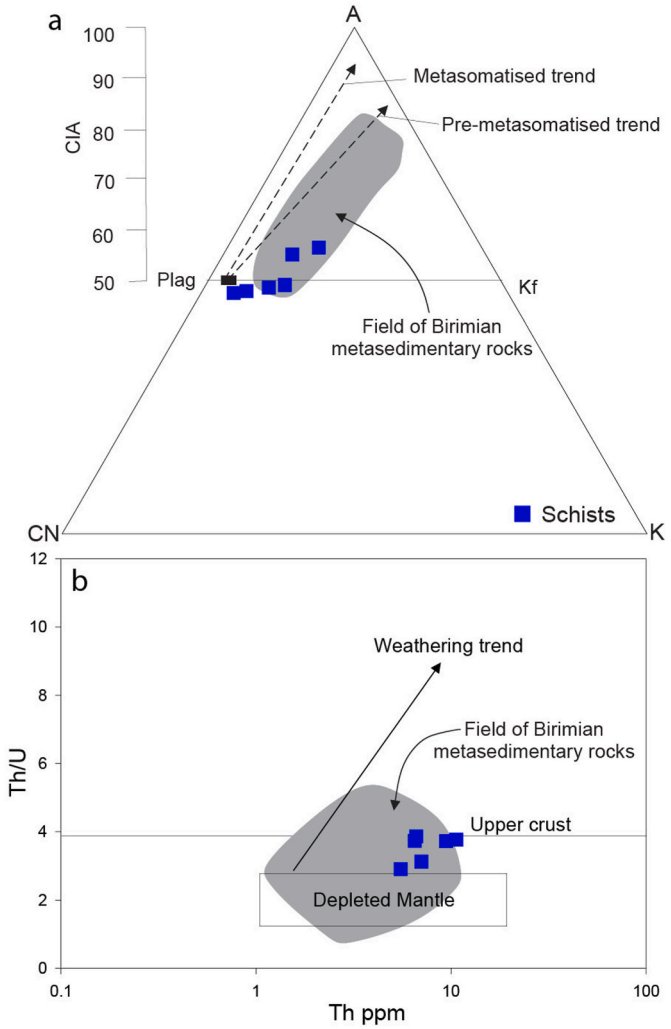

Fig. 14. (a) Al-CN-K and (b) Th vs Th/U diagrams for the schists to assess weathering intensity. Kibi data is from Sakyi et al. (2018) whereas N-MORB and E-MORB values are from Gale et al. (2013) and OIB values from Sun and McDonough (1989). Data for the field of Birimian metasedimentary rocks is from (Asiedu et al., 2007, 2009, 2017, 2019; Manu et al., 2013; Sakyi et al., 2019).

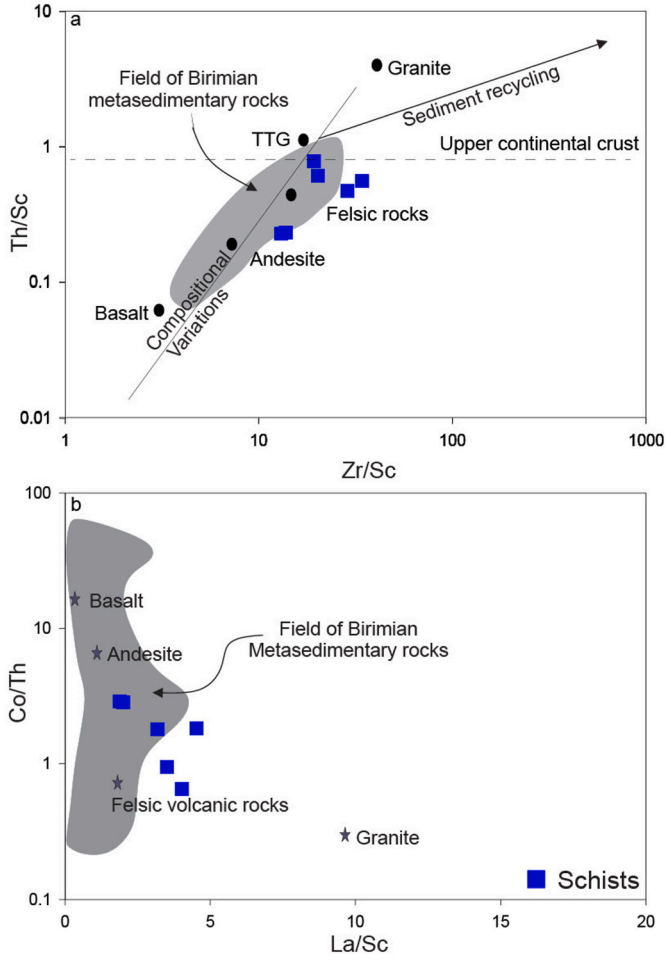

Fig. 15. (a) The La/Th-Hf Diagram (after Floyd and Leveridge (1987)) and (b) The Co/Th vs La/Sc Diagram (after McLennan and Taylor (1991) for the schists. Data for the field of Birimian metasedimentary rocks is from (Asiedu et al., 2007, 2009, 2019, 2017; Manu et al., 2013; Sakyi et al., 2019).

from subduction zone and exhibit signatures typical of Mid-Ocean ridge basaltic rocks and island arc tholeiitic basalts. The samples exhibiting non-arc characteristics could indicate source enrichment of a subduction zone component or sediment recycling.

Most tectonic settings with stable crust or recycled sediment exposures have Th/Sc values $\geq$ 1.0 (McLennan and Taylor, 1991). From Table 5, the low Th/Sc values of 0.23–0.79 indicate that the schists from the Suhum-Akwadum area formed in active tectonic settings, such as active continental margin. Verma and Armstrong-Altrin (2013) proposed two multidimensional discrimination diagrams (high-silica ((SiO_2)adj = 63–95 %) and low-silica ((SiO2)adj = 35–63 %)) in order to identify arc, rift, and collisional settings. On the high-silica diagram (Fig. 16c), the schists of the Suhum-Akwadum area are entirely plotted in the arc setting. This corroborates the fact that these samples were derived from an active continental margin setting. To further constrain the tectonic setting of the schists from the Suhum-Akwadum area, the La/Sc versus Ti/Zr tectonic discriminant diagram was plotted (Bhatia and Crook, 1986). The La/Sc versus Ti/Zr tectonic discriminant diagram (Fig. 16d) places the schists from the Suhum-Akwadum area mostly within the continental Island Arc setting akin to Birimian metasedimentary rocks, and a few samples sprawling within the active continental margin setting.

5. Implications for the crustal evolution of the Rhyacian Birimian terrane in Ghana

The Birimian Paleoproterozoic rocks were formed during the Rhyacian Eburnean event (Abouchami et al., 1990; Baratoux et al., 2011). The regional geochemical dataset indicates the involvement of subduction processes in their formation and evolution (Dampare et al., 2008; Senyah et al., 2016; Sakyi et al., 2018, 2020; McFarlane et al., 2019). The trace element signatures of the greenstones that make up the Birimian terrane show consistent negative Nb-Ta troughs, negative P and Ti anomalies, along with positive Pb anomalies, variable enrichment of LILE and depletion of HFSE typical of arc crust (Dampare et al., 2008; Senyah et al., 2016; Sakyi et al., 2018, 2020). The amphibolite of the Suhum-Akwadum area in Ghana were compared to other greenstone belts in the Birimian terrane, such as the Kibi belt. The amphibolite exhibit similar major and trace element characteristics as those of the Kibi belts. The greenstones from the Kibi belt are mainly classified as subalkaline basalts with low Mg# and Nb contents, resembling the amphibolite from the Suhum-Akwadum area of the Suhum Basin. The negative Nb-Ta peaks displayed by the greenstones from the Kibi belts suggest an arc-setting character, implying subduction zone processes for their formation (Fig. 7) (Sakyi et al., 2018). The Suhum-Akwadum area amphibolite may have been formed in a similar subduction zone setting as the greenstones from the Kibi belt as they display negative Nb-Ta

Table 4
Elemental ratios for the schists compared to sediments from felsic and mafic sources (Amstrong-Altrin et al., 2004).

	Schists from Suhum Basin	Range of sediments from felsic sources	Range of sediments from mafic sources
La/Sc	1.89–4.53	2.50–16.3	0.43–0.86
Th/Sc	0.23–0.79	0.84–20.5	0.05–0.22
Cr/Th	1.87–12.61	4.00–15.0	25.0–500
La/Co	2.78–10.98	0.67–19.4	0.04–1.40
Th/Co	0.35–1.53	1.80–13.8	0.14–0.38
Eu/Eu*	0.62–0.84	0.40–0.94	0.71–0.95
La/Lu	4.73–18.60	3.00–27.0	1.10–7.00

Table 5
Summary of geochemical characteristics of provenance types (after McLennan et al., 1993; 1995).

Terrane type	Eu/Eu*	Th/Sc	Other geochemical features	Description
Old Upper Continental Crust (OUC)	~0.60–0.70	~1.0	Evolved major element compositions (e.g. High Si/Al, CIA); High LILE abundances, uniform compositions.	Old igneous/metamorphic/sedimentary terranes affected intracrustal differentiation. Stable cratons, old foundation of active settings.
Recycled Sedimentary Rocks (RSR)	~0.60–0.70	≥1.0	Evidence of heavy mineral concentrations in trace elements (e.g. Zr, Hf for Zircon, REE for monazite).	Recycled sedimentary/metasedimentary rocks specifically identified. If not separately identified part of OUC.
Young Undifferentiated Volcanic Arc (YUA)	~1.0	<1.0	Unevolved major element compositions (e.g. Low Si/Al, CIA); High LILE abundances, variable compositions.	Young mantle-derived volcanic/plutonic arc rocks. Dominates forearcs, component in continental arcs, backarcs.
Young Differentiated Volcanic Arc (YUA)	~0.50–0.90	Variable	Evolved major element compositions (e.g. High Si/Al, CIA); High LILE abundances, variable compositions.	Young mantle-derived volcanic/plutonic arc rocks affected by intracrustal differentiation. Similar environments as YUA but more mature arcs or more dissection.

Various exotic components: Chemical signature depends on the nature of the component. For example, very high Mg, Cr, Ni, V and Cr/V would be distinctive of ophiolitic sources.

troughs, negative P and Ti anomalies, variable enrichment of LILE and depletion of HFSE. This is consistent with findings from the other greenstone belts of the Birimian terrane (Dampare et al., 2008; Senyah et al., 2016; Sakyi et al., 2018, 2020). Overall, our new and published geochemical data suggest that the greenstones of the Birimian terrane are related to a volcanic arc environment during the subduction-accretion process.

The available petrographic and geochemical, including Rb-Sr and Sm-Nd data for the metasedimentary rocks from the greenstone belts and metasedimentary basins indicate that these rocks were deposited in an active continental margin (Roddaz et al., 2007; Manu et al., 2013; Asiedu et al., 2017, 2019; Sakyi et al., 2019; Brako et al., 2022; Kazapoe et al., 2023). The deposition was characterised by subduction-accretion processes, and the sediments were sourced from the greenstone and granitoid-gneiss complexes of the Rhyacian Birimian terrane (Roddaz et al., 2007; Manu et al., 2013; Asiedu et al., 2017, 2019; Sakyi et al., 2019; Brako et al., 2022; Kazapoe et al., 2023). The geochemical signatures recorded in the studied schists from the Suhum-Akwadum area of the Suhum Basin are consistent with those reported in previous studies. This reflects low chemical weathering intensity, immature to moderately mature sediments and deposition in an active continental margin setting with sediments sourced from greenstone and granitoid-gneiss complexes of the Rhyacian Birimian terrane (Figs. 14 and 156c and 16d). Therefore, the current and previous geochemical data confirm the presence of an arc tectonic setting in the formation of the metasedimentary basins of the Birimian terrane.

Our findings thus support the subduction-accretion process model proposed for the evolution of the Birimian terrane of the West African Craton. According to the literature, sedimentation and volcanism occur simultaneously (Leube et al., 1990). Hence, active continental and arc signatures should be the most plausible results for greenstones and metasedimentary rocks, as in the case of this study. The overall geochemical data suggest that the greenstones and metasedimentary rocks formed during a single orogenic event related to an arc environment where subduction zone components contributed to the generation of their parental magmas and sedimentation. This finding is consistent with the onset of "modern-style" subduction-related processes during the Archean-Paleoproterozoic transitional period in the West African Craton. The finding, corroborated by Ganne et al. (2012), identified HP-LT blueschist Paleoproterozoic rocks (a hallmark of modern-style subduction) in the WAC.

6. Conclusions

The petrographical and geochemical data of metasedimentary rocks and amphibolite from the Suhum-Akwadum area of the Suhum Basin have been analysed with the following conclusions:

- The Suhum-Akwadum amphibolite are ortho-amphibolites, chemically resembling subalkaline basalts.
- They exhibit negative Nb-Ta, P, and Ti anomalies, low Nb/Th ratios, and LILE enrichment with HFSE depletion, signatures typical of subduction-related greenstones in the Birimian terrane, however, few samples show enriched characteristics.
- The schists are geochemically classified as shales and wackes, showing low weathering intensity (CIA <60, CIW <70) and derivation from greenstone and granitoid-gneiss sources.
- Their geochemical characteristics indicate deposition in an active continental margin, consistent with other Birimian metasedimentary basins formed in an arc setting.
- Overall data suggest both the amphibolite and metasedimentary rocks formed during a single orogenic event linked to a volcanic arc/subduction environment, reflecting the emergence of modern-style plate tectonics in the Archean–Paleoproterozoic transition in the WAC.

CRediT authorship contribution statement

Daniel Kwayisi: Writing – review & editing, Writing – original draft, Visualization, Validation, Supervision, Data curation, Conceptualization. **Susanna S. Boateng:** Writing – review & editing, Visualization, Methodology, Investigation, Formal analysis. **Naa A. Agra:** Writing – review & editing, Validation. **Solomon Anum:** Supervision, Resources, Investigation. **Raymond W. Kazapoe:** Writing – review & editing,

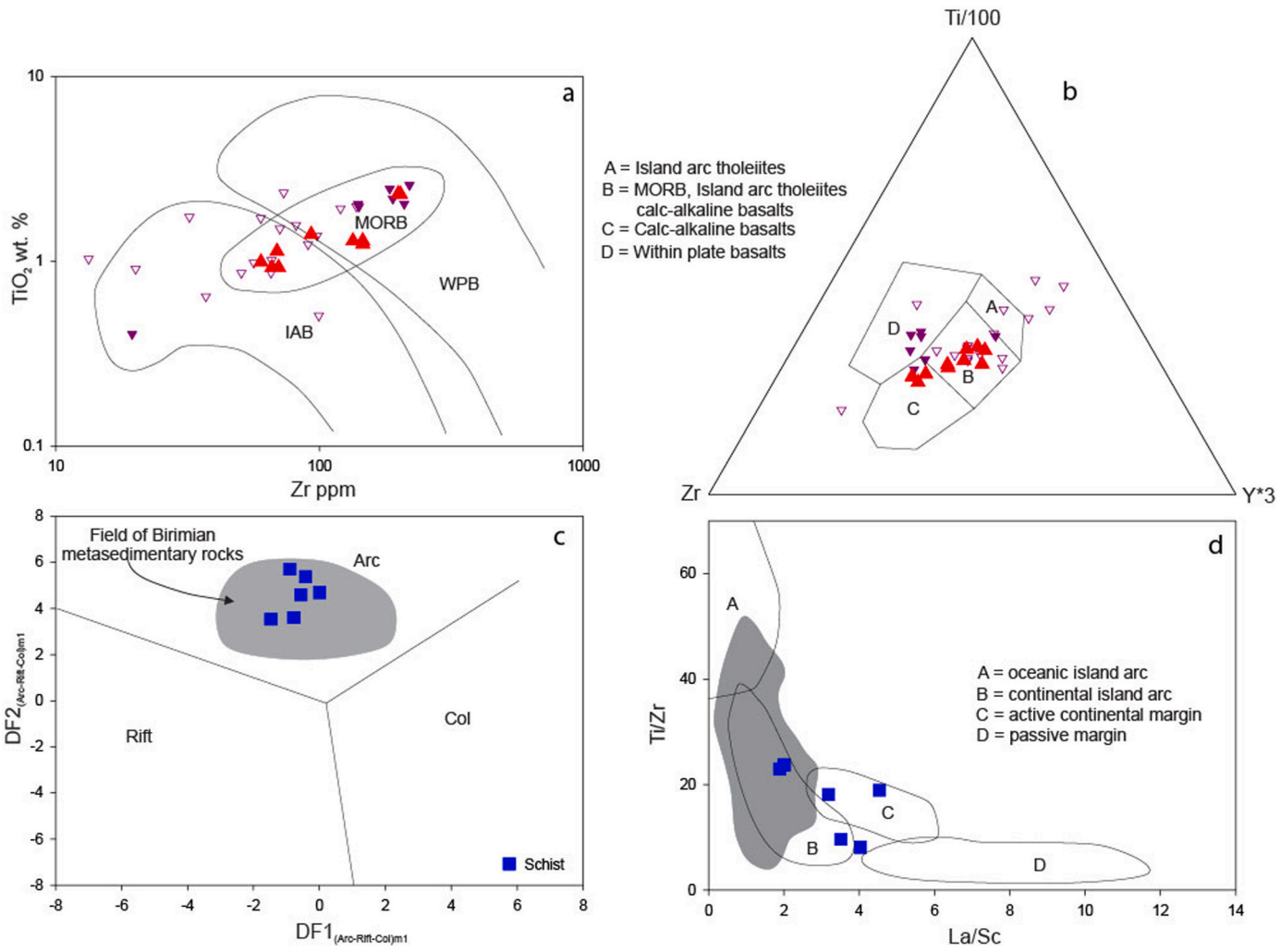

Fig. 16. Tectonic discrimination diagrams (a) Zr vs TiO2 (Floyd and Winchester, 1975), (b) Zr-Y*3-Ti/100 (Pearce and Cann, 1973), for the amphibolite (c) (SiO2) adj =<63 % discriminant function (Verma and Armstrong-Altrin, 2013) and (d) La/Sc vs Ti/Zr (Bhatia and Crook, 1986). Data for the field of Birimian metasedimentary rocks is from (Asiedu et al., 2007, 2009, 2019, 2017; Manu et al., 2013; Sakyi et al., 2019).

Writing – original draft, Visualization. **Abigail E. Ayikwei:** Writing – review & editing, Writing – original draft, Data curation. **Chris Y. Anani:** Writing – review & editing, Writing – original draft, Visualization, Data curation. **Daniel K. Asiedu:** Writing – review & editing, Writing – original draft, Supervision.

Declaration of competing interest

The authors declare that they have no known competing financial interests or personal relationships that could have appeared to influence the work reported in this paper.

Acknowledgement

The fieldwork in Ghana was enabled by the Ghana Geological Survey Authority. The corresponding author also thanks the Department of Earth Science Capacity Building for financial support during her graduate studies at the University of Ghana. We appreciate the reviewers and the handling editor for their time in reviewing and commenting on our manuscript.

Data availability

Data will be made available on request.

References

Abitty, E.K., Dampare, S.B., Nude, P.M., Asiedu, D.K., 2016. Geochemistry and petrogenesis of the K-rich 'Bongo-type'granitoids in the Paleoproterozoic Bole–Nangodi greenstone belt of Ghana. J. Afr. Earth Sci. 122, 47–62.

Abouchami, W., Boher, M., Michard, A., Albarede, F., 1990. A major 2.1 Ga event of mafic magmatism in West Africa: an early stage of crustal accretion. J. Geophys. Res. Solid Earth 95 (B11), 17605–17629.

Agra, N.A., Elburg, M.A., Vorster, C., 2023. Constraints on Paleoproterozoic crustal growth from Birimian Supergroup lavas of the Bui belt (Ghana) in the West African Craton. Precambr. Res. 384, 106926.

Agyei-Duodu, J., Loh, G.K., Hirdes, W., Boamah, K.O., Baba, M., Anokwa, Y.M., Asare, C., Brako-hiapa, E., Mensah, R.B., Okla, R., Toloczyki, M., Davis, D.W., Glück, S., 2009. Geological Map of Ghana 1:1 000 000. BGS/GGS, Accra, Ghana/Hannover,Germany, p. 1.

Amponsah, P.O., Kwayisi, D., Awunyo, E.K., Sapah, M.S., Sakyi, P.A., Su, B.X., Lu, Y., Nude, P.M., 2023. New evidence for crustal reworking and juvenile arc-magmatism during the Palaeoproterozoic Eburnean events in the Suhum Basin, South-east Ghana. Geol. J. 58 (10), 3734–3755.

Amstrong-Altrin, J.S., Lee, Y.I., Verma, S.P., Ramasamy, S., 2004. Geochemistry of sandstones from the Upper Miocene Kudankulam Formation, southern India: implications for provenance, weathering, and tectonic setting. J. Sediment. Res. 74, 285–297.

Anum, S., Sakyi, P.A., Su, B.-X., Nude, P.M., Nyame, F., Asiedu, D., Kwayisi, D., 2015. Geochemistry and geochronology of granitoids in the Kibi-Asamankese area of the Kibi-Winneba volcanic belt, southern Ghana. J. Afr. Earth Sci. 102, 166–179.

Asiedu, D., Dampare, S., Sakyi, P.A., Boamah, D., 2007. Major-and trace-element geochemistry of kimberlitic rocks in the akwatia area of the birim diamondiferous field, southwest ghana. Afr. J. Sci. Technol. 8 (2).

Asiedu, D., Kutu, J., Manu, J., Hayford, E., 2009. Geochemistry and provenance of metagreywackes from the Konongo area, Southwestern Ghana. Afr. J. Sci. Technol. 10 (1).
Armstrong-Altrin, J.S., Machain-Castillo, M.L., Rosales-Hoz, L., Carranza-Edwards, A., Sanchez-Cabeza, J.A., Ruíz-Fernández, A.C., 2015. Provenance and depositional history of continental slope sediments in the Southwestern Gulf of Mexico unraveled by geochemical analysis. Cont. Shelf Res. 95, 15–26.
Asiedu, D.K., Agoe, M., Amponsah, P.O., Nude, P.M., Anani, C.Y., 2019. Geochemical constraints on provenance and source area weathering of metasedimentary rocks from the Paleoproterozoic (~ 2.1 Ga) Wa-Lawra Belt, southeastern margin of the West African Craton. Geodin. Acta 31 (1), 27–39.
Asiedu, D.K., Asong, S., Atta-Peters, D., Sakyi, P.A., Su, B.-X., Dampare, S.B., Anani, C.Y., 2017. Geochemical and Nd-isotopic compositions of juvenile-type Paleoproterozoic Birimian sedimentary rocks from southeastern West African Craton (Ghana): constraints on provenance and tectonic setting. Precambr. Res. 300, 40–52.
Atanga, F., Amponsah, P.O., Nunoo, S., Kwayisi, D., Forson, E.D., Akabzaa, T.M., Nude, P.M., 2023. The geology and geochemistry of the Rhyacian Josephine gold deposit, Northwest Ghana. Appl. Earth Sci. 132 (3–4), 252–270.
Baratoux, L., Metelka, V., Naba, S., Jessell, M.W., Grégoire, M., Ganne, J., 2011. Juvenile Paleoproterozoic crust evolution during the Eburnean orogeny (~ 2.2–2.0 Ga), western Burkina Faso. Precambr. Res. 191 (1–2), 18–45.
Baratoux, L., Söderlund, U., Ernst, R., De Roever, E., Jessell, M., Kamo, S., Naba, S., Perrouty, S., Metelka, V., Yatte, D., 2019. New U–Pb baddeleyite ages of mafic dyke swarms of the West African and Amazonian cratons: implication for their configuration in supercontinents through time. Dyke swarms of the world: A modern perspective 263–314.
Bau, M., 1996. Controls on the fractionation of isovalent trace elements in magmatic and aqueous systems: evidence from Y/Ho, Zr/Hf, and lanthanide tetrad effect. Contrib. Mineral. Petrol. 123 (3), 323–333.
Bhatia, M.R., Crook, K.A., 1986. Trace element characteristics of graywackes and tectonic setting discrimination of sedimentary basins. Contrib. Mineral. Petrol. 92 (2), 181–193.
Blundy, J., Wood, B., 1994. Prediction of crystal–melt partition coefficients from elastic moduli. Nature 372 (6505), 452–454.
Boher, M., Abouchami, W., Michard, A., Albarede, F., Arndt, N.T., 1992. Crustal growth in west Africa at 2.1 Ga. J. Geophys. Res. Solid Earth 97 (B1), 345–369.
Brako, B.A., Amadu, C.C., Foli, G., Nude, P.M., Gawu, S.K., 2022. Petrography and geochemistry of metasedimentary rocks from the Paleoproterozoic Birimian at the Chagupana area, North-West Ghana: implications for provenance and tectonic setting. Arabian J. Geosci. 15 (24), 1749.
Condie, K.C., 1993. Chemical composition and evolution of the upper continental crust: contrasting results from surface samples and shales. Chem. Geol. 104 (1–4), 1–37.
Cullers, R.L., 1994. The controls on the major and trace element variation of shales, siltstones, and sandstones of Pennsylvanian-Permian age from uplifted continental blocks in Colorado to platform sediment in Kansas, USA. Geochem. Cosmochim. Acta 58 (22), 4955–4972.
Cullers, R.L., 1995. The controls on the major-and trace-element evolution of shales, siltstones and sandstones of Ordovician to Tertiary age in the Wet Mountains region, Colorado, USA. Chem. Geol. 123 (1–4), 107–131.
Cullers, R.L., 2002. Implications of elemental concentrations for provenance, redox conditions, and metamorphic studies of shales and limestones near Pueblo, CO, USA. Chem. Geol. 191 (4), 305–327.
Cullers, R.L., Basu, A., Suttner, L.J., 1988. Geochemical signature of provenance in sand-size material in soils and stream sediments near the Tobacco Root batholith, Montana, USA. Chem. Geol. 70 (4), 335–348.
Dampare, S., Shibata, T., Asiedu, D., Osae, S., Banoeng-Yakubo, B., 2008. Geochemistry of Paleoproterozoic metavolcanic rocks from the southern Ashanti volcanic belt, Ghana: petrogenetic and tectonic setting implications. Precambr. Res. 162 (3–4), 403–423.
Davis, D., Hirdes, W., Schaltegger, U., Nunoo, E., 1994. U- Pb age constraints on deposition and provenance of Birimian and gold-bearing Tarkwaian sediments in Ghana, West Africa. Precambr. Res. 67 (1–2), 89–107.
Elburg, M.A., 2010. Sources and Processes in Arc Magmatism: the Crucial Role of Water (An Inaugural Lecture to the Society). Geologica belgica.
Fitton, J.G., James, D., Kempton, P., Ormerod, D., Leeman, W., 1988. The role of lithospheric mantle in the generation of late Cenozoic basic magmas in the western United States. J. Petrol. (1), 331–349.
Floyd, P.A., Leveridge, B.E., 1987. Tectonic environment of the Devonian Gramscatho basin, south Cornwall: framework mode and geochemical evidence from turbiditic sandstones. J. Geol. Soc. 144 (4), 531–542.
Floyd, P.A., Winchester, J.A., 1975. Magma type and tectonic setting discrimination using immobile elements. Earth Planet Sci. Lett. 27 (2), 211–218.
Gale, A., Dalton, C.A., Langmuir, C.H., Su, Y., Schilling, J.G., 2013. The mean composition of ocean ridge basalts. G-cubed 14 (3), 489–518.
Gill, J.B., 2012. Orogenic Andesites and Plate Tectonics, 16. Springer Science & Business Media.
Ganne, J., De Andrade, V., Weinberg, R.F., Vidal, O., Dubacq, B., Kagambega, N., et al., 2012. Modern-style plate subduction preserved in the Palaeoproterozoic West African craton. Nat. Geosci. 5 (1), 60–65.
Hadji, F., Marok, A., Samet, A.M., Reolid, M., Bensefia, K.E., 2024. Inorganic geochemistry of Miocene sediments from the Lower Chelif Basin (NW Algeria) for approaching weathering and palaeoclimatic conditions. J. Iber. Geol. 50 (2), 137–156.
Harnois, L., 1988. The CIW index: a new chemical index of weathering. Sediment. Geol. 55 (3), 319–322.
Hayashi, K.-I., Fujisawa, H., Holland, H.D., Ohmoto, H., 1997. Geochemistry of~ 1.9 Ga sedimentary rocks from northeastern Labrador, Canada. Geochem. Cosmochim. Acta 61 (19), 4115–4137.
Hirdes, W., Davis, D., Lüdtke, G., Konan, G., 1996. Two generations of Birimian (Paleoproterozoic) volcanic belts in northeastern Côte d'Ivoire (West Africa): consequences for the 'Birimian controversy'. Precambr. Res. 80 (3–4), 173–191.
Herron, M.M., 1988. Geochemical classification of terrigenous sands and shales from core or log data. J. Sediment. Res. 58 (5), 820–829.
Hirdes, W., Davis, D.W., 1998. First U- Pb zircon age of extrusive volcanism in the Birimian Supergroup of Ghana/West Africa. J. Afr. Earth Sci. 27 (2), 291–294.
Hofmann, A., 2014. Sampling mantle heterogeneity through oceanic basalts: isotopes and trace elements. Treatise Geochem. 3, 67–101.
Hofmann, A.W., 1988. Chemical differentiation of the Earth: the relationship between mantle, continental crust, and oceanic crust. Earth Planet Sci. Lett. 90 (3), 297–314.
Jenner, G., Dunning, G., Malpas, J., Brown, M., Brace, T., 1991. Bay of Islands and Little Port complexes, revisited: age, geochemical and isotopic evidence confirm suprasubduction-zone origin. Can. J. Earth Sci. 28 (10), 1635–1652.
Jung, C., Jung, S., Hoffer, E., Berndt, J., 2006. Petrogenesis of Tertiary mafic alkaline magmas in the Hocheifel, Germany. J. Petrol. 47 (8), 1637–1671.
Kazapoe, R.W., Okunlola, O., Arhin, E., Olisa, O., Kwayisi, D., Dzikunoo, E.A., Amuah, E. E.Y., 2023. Compositional characteristics of mineralised and unmineralised gneisses and schist around the Abansuoso area, southwestern Ghana. Appl. Earth Sci. 132 (1), 36–51.
Kazapoe, W.R., Okunlola, O., Arhin, E., Olisa, O., Harris, C., Kwayisi, D., Torkorno, S., Amuah, E.E.Y., 2022. Geology and isotope systematics of gold deposits in the abansuoso area of the sefwi belt, southwestern Ghana. Geol. Ecol. Landsc. 1–22.
Kouamelan, A.N., Djro, S.C., Allialy, M.E., Paquette, J.-L., Peucat, J.-J., 2015. The oldest rock of Ivory Coast. J. Afr. Earth Sci. 103, 65–70.
Kwayisi, D., Elburg, M., Lehmann, J., 2022a. Preserved ancient oceanic lithosphere within the Buem structural unit at the eastern margin of the West African Craton. Lithos 410, 106585.
Kwayisi, D., Lehmann, J., Elburg, M., 2022b. Provenance and depositional setting of the Buem structural unit (Ghana): implications for the paleogeographic reconstruction of the West African and Amazonian cratons in Rodinia. Gondwana Res. 109, 183–204.
Kwayisi, D., Nyavor, E., Dzikunoo, E.A., Fynn, I.E.M., Kutu, J., Nude, P.M., 2023. Cryogenian-Ediacaran crustal growth and evolution of the active margin of the Dahomeyide belt, Ghana. Geol. Mag. 160 (10), 1914–1931.
Kwayisi, D., Amponsah, P.O., Agra, N.A., Nunoo, S., Thompson, J., Kazapoe, R.W., Asiedu, D., Nude, P.M., 2024. Neoproterozoic passive margin formation and evolution during the Rodinia–Gondwana supercontinent cycle at the eastern margin of the West African Craton. Geol. Mag. 161, e14.
Kwayisi, D., Amponsah, P.O., Awunyo, E.K., Sapah, M.S., Sakyi, P.A., Su, B.X., Nude, P. M., Ayikwei, A.E., Forson, E.D., 2025. Petrology and geochemistry of the Suhum Basin granitoid complex, Ghana: implications for crustal growth during the Rhyacian orogeny of the West African Craton. J. Afr. Earth Sci. 222, 105475.
Lai, S., Qin, J., Li, Y., Li, S., Santosh, M., 2012. Permian high Ti/Y basalts from the eastern part of the Emeishan Large Igneous Province, Southwestern China: petrogenesis and tectonic implications. J. Asian Earth Sci. 47, 216–230.
Leube, A., Hirdes, W., Mauer, R., Kesse, G.O., 1990. The early Proterozoic Birimian Supergroup of Ghana and some aspects of its associated gold mineralization. Precambr. Res. 46 (1–2), 139–165.
Manikyamba, C., Ganguly, S., Santosh, M., Saha, A., Chatterjee, A., Khelen, A.C., 2015. Neoarchean arc–juvenile back-arc magmatism in eastern Dharwar Craton, India: geochemical fingerprints from the basalts of Kadiri greenstone belt. Precambr. Res. 258, 1–23.
Manikyamba, C., Pahari, A., Singh, T.D., Chatterjee, A., Ganguly, S., 2020. Evolution of geodynamic processes in Neoarchean Kadiri greenstone belt, eastern Dharwar Craton, India: implications on the migrating arc magmatism. J. Geodyn. 136, 101717.
Manu, J., Asiedu, D.K., Anani, C.Y., 2013. Geochemistry of Birimian phyllites from the Obuasi and Prestea Mines, Southwestern Ghana: implications for provenance and source-area weathering. Int. J. Basic Appl. Sci. 2 (1), 12.
McDonough, W.F., Rudnick, R.L., 1998. Mineralogy and composition of the upper mantle. Rev. Mineral. 37, 139–164.
McFarlane, H., Ailleres, L., Betts, P., Ganne, J., Baratoux, L., Jessell, M., Block, S., 2019. Episodic collisional orogenesis and lower crust exhumation during the Palaeoproterozoic Eburnean Orogeny: evidence from the Sefwi Greenstone Belt, West African Craton. Precambr. Res. 325, 88–110.
McLennan, S., Taylor, S., 1991. Sedimentary rocks and crustal evolution: tectonic setting and secular trends. J. Geol. 99 (1), 1–21.
McLennan, S.M., Hemming, S., McDaniel, D.K., Hanson, G.N., 1993. Geochemical Approaches to Sedimentation, Provenance, and Tectonics.
McLennan, S.M., Hemming, S.R., Taylor, S.R., Eriksson, K.A., 1995. Early Proterozoic crustal evolution: geochemical and NdPb isotopic evidence from metasedimentary rocks, southwestern North America. Geochem. Cosmochim. Acta 59 (6), 1153–1177.
Mclennan, S.M., 2018. Rare earth elements in sedimentary rocks: influence of provenance and sedimentary processes. In: Geochemistry and Mineralogy of Rare Earth Elements. De Gruyter, pp. 169–200.
Nagarajan, R., Madhavaraju, J., Nagendra, R., Armstrong-Altrin, J.S., Moutte, J., 2007. Geochemistry of Neoproterozoic shales of the Rabanpalli Formation, Bhima Basin, Northern Karnataka, southern India: implications for provenance and paleoredox conditions. Revista mexicana de ciencias geológicas 24 (2), 150–160.
Nance, W., Taylor, S., 1977. Rare earth element patterns and crustal evolution—II. Archean sedimentary rocks from Kalgoorlie, Australia. Geochem. Cosmochim. Acta 41 (2), 225–231.

Nesbitt, H., Young, G., 1982. Early Proterozoic climates and plate motions inferred from major element chemistry of lutites. Nature 299, 715–717.
Nude, P.M., Kwayisi, D., Taki, N.A., Kutu, J.M., Anani, C.Y., Banoeng-Yakubo, B., Asiedu, D.K., 2015. Petrography and chemical evidence for multi-stage emplacement of western Buem volcanic rocks in the Dahomeyide orogenic belt, southeastern Ghana, West Africa. J. Afr. Earth Sci. 112, 314–327.
Nunoo, S., Hofmann, A., Kramers, J., 2022. Geology, zircon u–pb dating and εhf data for the julie greenstone belt and associated rocks in nw Ghana: implications for birimian-to-tarkwaian correlation and crustal evolution. J. Afr. Earth Sci. 186, 104444.
Nyame, F., 2008. Petrography and geochemistry of intraclastic manganese–carbonates from the∼ 2.2 Ga Nsuta deposit of Ghana: significance for manganese sedimentation in the Palaeoproterozoic of West Africa. J. Afr. Earth Sci. 50 (2–4), 133–147.
Nyame, F., Beukes, N., 2006. The genetic significance of carbon and oxygen isotopic variations in Mn-bearing carbonates from the Palaeo-Proterozoic (∼ 2.2 GA) Nsuta deposit in the Birimian of Ghana. Carbonates Evaporites 21, 21–32.
Pearce, J.A., Cann, J.R., 1973. Tectonic setting of basic volcanic rocks determined using trace element analyses. Earth Planet Sci. Lett. 19 (2), 290–300.
Pearce, J.A., Peate, D.W., 1995. Tectonic implications of the composition of volcanic arc magmas. Annu. Rev. Earth Planet Sci. 23 (1), 251–285.
Pearce, N.J., 2014. Towards a protocol for the trace element analysis of glass from rhyolitic shards in tephra deposits by laser ablation ICP-MS. J. Quat. Sci. 29 (7), 627–640.
Pearce, J.A., Wyman, D.A., 1996. A user's guide to basalt discrimination diagrams. In: Trace element geochemistry of volcanic rocks: applications for massive sulphide exploration, Vol. 12. Geological Association of Canada. Short Course Notes, pp. 79–113.
Peate, D.W., Hawkesworth, C.J., Mantovani, M.M., Rogers, N.W., Turner, S.P., 1999. Petrogenesis and stratigraphy of the high-Ti/Y Urubici magma type in the Paraná flood basalt province and implications for the nature of 'Dupal'-type mantle in the South Atlantic region. J. Petrol. 40 (3), 451–473.
Reichow, M.K., Saunders, A., White, R., Al'Mukhamedov, A., Medvedev, A.Y., 2005. Geochemistry and petrogenesis of basalts from the West Siberian Basin: an extension of the Permo–Triassic Siberian Traps, Russia. Lithos 79 (3–4), 425–452.
Roddaz, M., Christophoul, F., Zambrano, J.D.B., Soula, J.-C., Baby, P., 2012. Provenance of late Oligocene to quaternary sediments of the Ecuadorian Amazonian foreland basin as inferred from major and trace element geochemistry and Nd–Sr isotopic composition. J. S. Am. Earth Sci. 37, 136–153.
Roddaz, M., Debat, P., Nikiéma, S., 2007. Geochemistry of Upper Birimian sediments (major and trace elements and Nd–Sr isotopes) and implications for weathering and tectonic setting of the Late Paleoproterozoic crust. Precambr. Res. 159 (3–4), 197–211.
Rollinson, H., 2016. Archaean crustal evolution in West Africa: a new synthesis of the Archaean geology in Sierra Leone, Liberia, Guinea and Ivory Coast. Precambr. Res. 281, 1–12.
Rudnick, R., 2005. Composition of the continental crust. Crust Treatise Geochem. 3, 17–18.
Sakyi, P.A., Anum, S., Su, B.X., Nude, P.M., Su, B.C., Asiedu, D.K., Nyame, F., Kwayisi, D., 2018. Geochemical and Sr-Nd isotopic records of Paleoproterozoic metavolcanics and mafic intrusive rocks from the West African Craton: evidence for petrogenesis and tectonic setting. Geol. J. 53 (2), 725–741.
Sakyi, P.A., Manu, J., Su, B.X., Kwayisi, D., Nude, P.M., Dampare, S.B., 2019. Geochemical and Sm–Nd isotopic evidence for the composition of the Palaeoproterozoic crust of the West African Craton in Ghana. Geol. J. 54 (6), 3940–3957.
Sakyi, P.A., Su, B.-X., Anum, S., Kwayisi, D., Dampare, S.B., Anani, C.Y., Nude, P.M., 2014. New zircon U–Pb ages for erratic emplacement of 2213–2130 Ma Paleoproterozoic calc-alkaline I-type granitoid rocks in the Lawra Volcanic Belt of Northwestern Ghana, West Africa. Precambr. Res. 254, 149–168.
Sakyi, P.A., Su, B.-X., Manu, J., Kwayisi, D., Anani, C.Y., Alemayehu, M., Malaviarachchi, S.P., Nude, P.M., Su, B.-C., 2020. Origin and tectonic significance of the metavolcanic rocks and mafic enclaves from the Palaeoproterozoic Birimian Terrane, SE West African Craton, Ghana. Geol. Mag. 157 (8), 1349–1366.
Sakyi, P.A., Kwayisi, D., Nunoo, S., Ocran, E., Su, B.X., Malaviarachchi, S.P., 2024. Crustal evolution of alternating Paleoproterozoic belts and basins in the Birimian terrane in southeastern West African Craton. J. Afr. Earth Sci. 220, 105449.
Saunders, A., Norry, M., Tarney, J., 1988. Origin of MORB and chemically-depleted mantle reservoirs: trace element constraints. J. Petrol. (1), 415–445.
Sedziafa, V., Song, Y., Sunkari, E.D., Kwayisi, D., Anani, C.Y., Asiedu, D.K., 2025. Provenance and source area weathering of sandstones from the Tarkwaian Group at the northeastern extent of the Paleoproterozoic Ashanti Belt, Ghana: constraints from petrography and geochemistry. J. Afr. Earth Sci. 224, 105536.
Senyah, G.A., Dampare, S.B., Asiedu, D.K., 2016. Geochemistry and tectonic setting of the Paleoproterozoic metavolcanic rocks from the Chirano Gold District, Sefwi belt, Ghana. J. Afr. Earth Sci. 122, 32–46.
Song, X.-Y., Zhou, M.-F., Hou, Z.-Q., Cao, Z.-M., Wang, Y.-L., Li, Y., 2001. Geochemical constraints on the mantle source of the upper Permian Emeishan continental flood basalts, southwestern China. Int. Geol. Rev. 43 (3), 213–225.
Sun, S.-S., McDonough, W.F., 1989. Chemical and isotopic systematics of oceanic basalts: implications for mantle composition and processes. Geological Society 42 (1), 313–345. London, Special Publications.
Tarney, J., 1977. PETROLOGY, mineralogy, and geochemistry OF the falkland plateau basement rocks, site 330. DEEP SEA DRILLING PROJECT.
Taylor, S.R., McLennan, S.M., 1985. The Continental Crust: Its Composition and Evolution.
Van Westrenen, W., Blundy, J.D., Wood, B.J., 2001. High field strength element/rare earth element fractionation during partial melting in the presence of garnet: implications for identification of mantle heterogeneities. G-cubed 2 (7).
Verma, S.P., Armstrong-Altrin, J.S., 2013. New multi-dimensional diagrams for tectonic discrimination of siliciclastic sediments and their application to Precambrian basins. Chem. Geol. 355, 117–133.
Verma, S.P., Armstrong-Altrin, J.S., 2016. Geochemical discrimination of siliciclastic sediments from active and passive margin settings. Sediment. Geol. 332, 1–12.
White, R., McKenzie, D., 1995. Mantle plumes and flood basalts. J. Geophys. Res. Solid Earth 100 (B9), 17543–17585.
Winchester, J., Max, M., 1982. The geochemistry and origins of the Precambrian rocks of the Rosslare Complex, SE Ireland. J. Geol. Soc. 139 (3), 309–319.
Winter, J.D., 2001. An Introduction to Igneous and Metamorphic Petrology *(No Title)*.
Xu, Y.-G., Ma, J.-L., Frey, F.A., Feigenson, M.D., Liu, J.-F., 2005. Role of lithosphere–asthenosphere interaction in the genesis of Quaternary alkali and tholeiitic basalts from Datong, western North China Craton. Chem. Geol. 224 (4), 247–271.
Yang, Q.Y., Ganguly, S., Shaji, E., Dong, Y., Nanda-Kumar, V., 2019. Extensional collapse of the Gondwana orogen: evidence from Cambrian mafic magmatism in the Trivandrum Block, southern India. Geosci. Front. 10 (1), 263–284.
Yaxley, G.M., 2000. Experimental study of the phase and melting relations of homogeneous basalt+ peridotite mixtures and implications for the petrogenesis of flood basalts. Contrib. Mineral. Petrol. 139 (3), 326–338.